NTNU
Det skapende universitet

Kompleksdannere under våtkjemisk syntese av oksider

Susanne Linn Skjærvø

Nanoteknologi
Innlevert: juni 2013
Hovedveileder: Mari-Ann Einarsrud, IMTE
Medveileder: Tor Grande, IMTE

Norges teknisk-naturvitenskapelige universitet
Institutt for materialteknologi

Oppgavetekst

Våtkjemiske syntesemetoder som sol-gel metoden benyttes for å framstille keramiske oksidmaterialer av høy kvalitet. Ved denne metoden blandes kationene som inngår i materialet i en homogen vandig løsning og denne homogeniteten opprettholdes i det faste oksidmaterialet ved at kationene bindes i en gel underveis i prosessen. For å stabilisere kationene i løsning benyttes forskjellige komplekseringsmidler. Selv om denne metoden i prinsippet skal gi et homogent enfase-materiale har vi erfart at for enkelte komplekse oksider får vi en utfelling av sekundære faser. Vi tror dette skyldes forskjellig grad av kompleksering av forskjellige typer kationer for et gitt komplekseringsmiddel. Vi ønsker derfor å benytte våre kunnskaper innen uorganisk kjemi til å studere hvilke komplekseringsmidler som best komplekserer forskjellige typer av kationer og på denne måten kunne gi generelle retningslinjer for hva slags komplekseringmiddel som anbefales benyttet til forskjellige oksidmaterialer. Denne prosjektoppgaven går derfor ut på å studere bruken av komplekseringsmidler med forskjellige funksjonelle grupper (-OH, -COOH, -C=O, etc) og disses omgivelser for å framstille et utvalg av oksider. Disse oksidene blir valgt slik at de består av kationer av forskjellig type (som danner basiske, sure eller amfotære oksider og kationer som karakteriseres som typisk harde og myke). Aktuelle materialer er $CuAlO_2$ som er et transparent ledende oksid samt Eu-dopet $NaLn(WO_4)_{2-x}(MoO_4)_x$ som er et fotoluminescerende materiale. Komplekseringen av kationene vil bli studert ved bruk av infrarød spektroskopi og røntgendiffraksjon. Hvorvidt enfase-materialer uten sekundære faser kan framstilles studeres ved hjelp av røntgendiffraksjon. Partikkelstørrelse og morfologi vil bli bestemt ved røntgendiffraksjon, SEM og nitrogen adsorpsjon. Utvalgte funksjonelle egenskaper til materialene vil også bli studert.

Abstract

The effect of different complexing agents in the modified Pechini method has been studied using malonic, malic and tartaric acid for the production of delafossite $CuAlO_2$ and malic and tartaric acid for the synthesis of $NaLa(WO_4)(MoO_4)$ with the scheelite structure.

The precursors $Cu(CH_3COO)_2 \cdot H_2O$ and $Al(NO_3)_3 \cdot 9\ H_2O$ were used for producing the gels of $CuAlO_2$. The amount of complexing agent, ethylene glycol and hot-plate temperature during evaporation of the solutions were varied. The gels became more amorphous and less metallic copper could be seen when EG was added to the solutions. The gels were calcined in air at 500, 600, 900, 1000 and 1150 ^oC and in nitrogen at 600, 800 and 1000 ^oC giving delafossite $CuAlO_2$ with $CuAl_2O_4$ and CuO impurities for 1150 ^oC in air while traces of delafossite $CuAlO_2$ could be seen in addition to metallic copper and γ-Al_2O_3 when calcined at 800 ^oC in nitrogen for a gel with the low amounts of complexing and polymerizing groups. The highest p-type conductivity measured for the $CuAlO_2$ powders calcined at 1150 ^oC and pressed into pellets was $3.1 \cdot 10^{-3}$ S cm^{-1} for powders made with high concentration of complexing agent.

Gels of Eu-doped $NaLa(WO_4)(MoO_4)$ were synthesized with $NaNO_3$ (s), $La(NO_3)_3 \cdot 6\ H_2O$, H_2WO_4, $(NH_4)_6Mo_7O_{24} \cdot 4\ H_2O$ and $Eu(NO_3)_3 \cdot 6\ H_2O$ as precursors and had a lower degree of crystallinity when EG was added to the solutions and for tartaric acid as complexing agent. The gels were calcined at 300, 400, 500, 600 and 1000 ^oC in air giving single-phase nanocrystalline $NaLa(WO_4)(MoO_4)$ for 600 and 1000 ^oC. Small amounts of the $NaLa(WO_4)(MoO_4)$ phase could be found at 400 ^oC and only traces of impurities could be found at 500 ^oC in addition to the $NaLa(WO_4)(MoO_4)$ phase. The photoluminescence emission characteristics showed to be quite satisfying for all the powders calcined at 600 and 1000 ^oC with a strong emission line at 615 nm.

Sammendrag

Effekten av ulike komplekseringsmidler i den modifiserte Pechini-metoden har blitt studert ved å benytte malon-, eple- og vinsyre under syntesen $CuAlO_2$ med delafossittstruktur og eple- og vinsyre for $NaLa(WO_4)(MoO_4)$ med scheelittstruktur.

Forløperne $Cu(CH_3COO)_2 \cdot H_2O$ og $Al(NO_3)_3 \cdot 9\,H_2O$ ble brukt i syntesen av $CuAlO_2$ sammen med varierende mengde komplekseringsmiddel og etylenglykol (EG). Kokeplatetemperaturen under innkoking av løsningen ble også variert. De resulterende gelene viste mindre krystallinitet og tilstedeværelse av metallisk kobber når EG ble tilsatt. Gelene ble kalsinert i luft ved 500, 600, 900, 1000 og 1150 ^{o}C og i nitrogen ved 600, 800 og 1000 ^{o}C. Alle gelene kalsinert ved 1150 ^{o}C i luft ga $CuAlO_2$ med delafossittstruktur med urenheter av $CuAl_2O_4$ og CuO. Spor av $CuAlO_2$ med delafossittstruktur ble også funnet i tillegg til metallisk kobber og γ-Al_2O_3 etter kalsinering i nitrogen ved 800 ^{o}C for den gelen med lavest mengde av komplekserende- og polymeriserende grupper. Den høyeste elektriske konduktiviteten for $CuAlO_2$ ble målt på en pellet presset av pulvere lagd med mye komplekseringsmiddel og kalsinert ved 1150 ^{o}C, og var $3.1{\cdot}10^{-3}$ S cm^{-1}.

Geler laget for å produsere $NaLa(WO_4)(MoO_4)$ ble syntetisert av forløperne $NaNO_3$ (s), $La(NO_3)_3{\cdot}\,6\,H_2O$, H_2WO_4, $(NH_4)_6Mo_7O_{24} \cdot 4\,H_2O$ og $Eu(NO_3)_3{\cdot}\,6\,H_2O$ og disse viste en lavere grad av krystallinitet ved tilsats av EG og ved bruk av vinsyre som komplekseringsmiddel. Gelene ble kalsinert ved 300, 400, 500, 600 og 1000 ^{o}C i luft. En-fase nanokrystallinsk $NaLa(WO_4)(MoO_4)$ ble dannet ved 600 og 1000 ^{o}C. Spor av den ønskede fasen ble funnet etter kalsinering ved 400 ^{o}C og få urenheter ble funnet etter kalsinering ved 500 ^{o}C i tillegg til $NaLa(WO_4)(MoO_4)$-fasen. Fotoluminescens-egenskapene var tildels tilfredsstillende for alle pulverene kalsinert ved 600 og 1000 ^{o}C med en sterk emisjonslinje ved 615 nm.

Preface

This report is the result of the work in connection with my master thesis (TMT4910), carried out during the 10th semester of the sivil engineering program for nanotechnology at the Norwegian University of Science and Technology. A synthesis method for two oxides has been studied, $CuAlO_2$ and Eu-doped $NaLa(WO_4)(MoO_4)$ and thus this work is a continuation of the preliminary master thesis ("the fall project") during the 9th semester [1]. Some results from this work have been included in this report as they complement the results obtained during this work. Eu-doped $NaLa(WO_4)(MoO_4)$ gels were produced in excessive amounts during the preliminary master thesis work and these were therefore used during this work as well.

Quite extensive quantities of laboratory work have been executed for achieving the required understanding of the relevant systems. During this work, several persons have been of great importance. My twin sister Sandra Helen Skjærvø has been a great support both academically and personally. Malin Sletnes has been a great advisor on the synthesis and characterization of $NaLa(WO_4)(MoO_4)$. Parts of the synthesis route of the $NaLa(WO_4)(MoO_4)$ have been inspired by the work of Vanesa Gil *et al.* on $La_{28-x}W_{4+x}O_{54+3x/2}$ [2] while the work of Selbach *et al.* on $BiFeO_3$ [3] and Li *et al.* on $CuAlO_2$ [4] have been of great influence on the synthesis of $CuAlO_2$. Julian Tolchard has provided excellent help on X-ray diffraction issues, both on setup and analysis. The Solar research group at the department of Materials Science and Engineering, including professor Tor Grande, has given me great input for a broader perspective and answers to complex problems during our weekly meetings. The greatest assistance has still been provided by my main supervisor Mari-Ann Einarsrud who

posesses impressing amounts of knowledge on many different topics and always believes in my abilities and pushes me to fulfill my potential. I wish to give a great acknowledgement to her for giving me this opportunity.

Contents

Part I
Introduction

1 Motivation

Wet chemical synthesis methods have many advantages compared to solid state methods. Normally, a lower synthesis temperature can be obtained giving a lower degree of agglomeration and aggregation of the particles and the easy mixing of precursors at a molecular level gives a very high degree of homogeneity in the product. Solid state methods may also include several steps of mechanical particle size reduction which may introduce defects and impurities to the material [5]. Such impurities may degrade the properties of the material, e.g. secondary phases may give contributions to the optical spectrum or affect the electrical conductivity of the material. In doped materials the degree of homogeneity is especially important as local areas with higher or lower concentration of dopants will give varying doping properties throughout the material. The presence of a solvent will give a better mixing of the present cations, but it may also result in an impurity problem as the solvent may be hard to remove from the powder. In the *Pechini method*, the synthesis method being studied in this report, hydroxylic acids are being added to the synthesis to enhance the homogeneity of the product [6], but these can also be challenging as they will set a lower boundary on the calcination temperature [5].

Nano-sized powders as a basis for making dense ceramic materials will often give advantages compared to powders of larger particles. The small particle size will make the powders easier to pack into dense objects and both the strength and hardness will thus be enhanced [7] along with in-

creased specific heat capacity, improved thermal expansion properties, lower thermal conductivity and improved magnetic properties [8]. Their ductility will also be better as superplasticity will occur [9].

1.1 $CuAlO_2$ as a p-type transparent conducting oxide

There are many obvious ways of exploiting *transparent conductive oxides* (TCO) in every-day applications as they are able to conduct electrical current while letting visible light pass through them. Improved flat-panel displays, UV light-emitting diodes, heterojunctions for solar cells, transparent semiconductor devices such as transistors, thermoelectric converters and sensing devices are just some of the possible applications [10, 11, 12, 13, 14]. TCOs would be even more useful if transparent p-n junctions were available, but today only n-type TCOs exists with satisfying conductivity. The oxide $CuAlO_2$ should in theory be ideal for making a p-type TCO with the desired conductivity [15]. Transparent p-n junctions could be employed in so-called "functional" windows which transmits the visible part of the solar radiation while generating electricity by the absorption of the ultra violet (UV) part. By employing this in solar cells, the absorption spectrum of the incident radiation is extended into the higher energy range to improve the cell efficiency. According to recent advances in the field of nanotechnology, tremendous opportunities in the optoelectronics industry are offered because of the drastic difference of the optical properties of the nanocrystals compared to the respective bulk materials. These properties are related to the nanosize and surface chemistry of the nanomaterials and explained in terms of quantum confinement effects [16]. This makes research with the aim of finding a good p-type TCO very important for future progress in completely transparent nanoactive devices, which may give a new dimension to the field of transparent electronics.

To make a good TCO, several requirements have to be fulfilled. The bandgap needs to be larger than 3.1 eV [14] to make the material transparent, but there has to be enough charge carriers present (holes in p-type conductors) to conduct a current. Excess charge carriers are produced by introducing non-stoichiometry and (or) appropriate dopants in a controlled manner. Acceptor or donor levels are then contributing to the conductivity by letting the charge carriers be excited more easily to levels where they can conduct current. A schematic representation of the bandgap for transparent conductors is shown in Figure 1.1. Photons in this visible energy range (2.1-3.1 eV) would normally not be able to excite electrons or holes, but the donor and acceptor levels make this possible. The right part of Figure 1.1 is giving the transmittance of the TCO with respect to incident radiation.

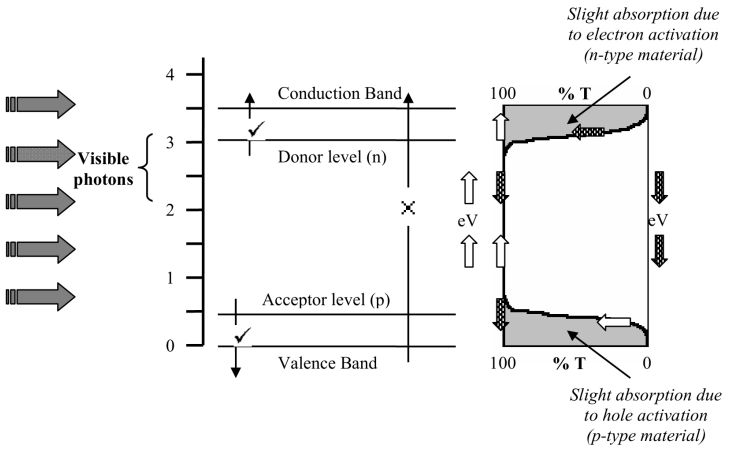

Figure 1.1: *Bandgap design for transparent conductors indicating the different energy levels. On the right is the transmittance of the TCO with respect to incident radiation. [14].*

The white arrows indicates the transmittance graph for a p-type TCO, where a slight absorption can be observed at low energies due to the activation of holes from acceptor level to VB. Similarly, the black arrows indicates the same for n-type TCO.

Among the p-type TCOs which have emerged, films of $CuAlO_2$ not only have a high transmittance in the visible region and an excellent conductivity [11], but also have good photovoltaic [17], ozone sensing [18], field-emission [19], thermoelectric [20] and photo-catalytic [21] properties.

1.2 $NaLa(WO_4)(MoO_4)$:Eu as a novel red phosphor

With the steadily protruding environmental challenges in our society, the traditional techniques of making white light does not satisfy the need to be energy efficient, as they rely on either discharge from gases or heat. Both phenomena are associated with large energy losses which occur because of the high temperatures and large Stokes shifts involved [22]. Phosphor-converted white light-emitting diodes (pc-WLEDs) are an energy efficient alternative to the conventional lighting sources. Figure 1.2 [23] represents three different ways of producing white light with LEDs: A) red+green+blue LEDs, B) UV-LED + red-green-blue phosphors, and C) blue-LED + yellow phosphor [23]. Method B) is assumed to be the best way of the three as it gives a high color rendering index, high chromatic stability under different driving currents and a tunable color temperature, but the disadvantages includes complex blending of different phosphors and a lack of an efficient red phosphor [24, 25]. The last point here is the reason for this work on $NaLa(WO_4)(MoO_4)$ as it has shown to be a promising host material for a novel red phosphor [26, 27].

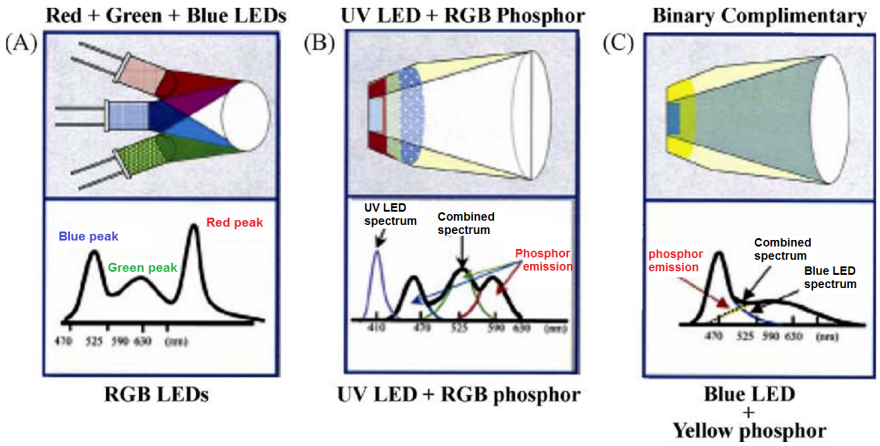

Figure 1.2: *Three ways of making white light based on LEDs where A) one red, green and blue (RGB) LED is put together to create white light, B) is using an ultraviolet (UV) LED to stimulate RGB phosphors and C) is using a blue LED that excites a yellow-emitting phosphor embedded in the epoxy dome; the combination of blue and yellow light makes a white-emitting LED [23].*

2 Aim of this work

Previously, $CuAlO_2$ has been succesfully made with the Pechini method [6]. Several precursors and calcination temperatures have been employed [4, 28, 29] by others, but the usage of other "citric acid-like" complexing agents has not been thoroughly investigated. Malonic acid, malic acid and tartaric acid are all quite similar to citric acid and the main goal of this work was to see if there could be found any differences in the products formed when using each of these three complexing agents. The amount of complexing agents and also the amount of the polymerization agent, ethylene glycol, could also give variations in the products. The effect of the hot-plate temperature and calcination temperature and atmosphere was

also investigated for the different samples. The aim of the work would be to find the best synthesis parameters for making nanocrystalline and homogeneous $CuAlO_2$ with this synthesis method using the metal cation precursors copper acetate and aluminium nitrate.

Eu-doped $NaLa(WO_4)(MoO_4)$ has, as far as the author is aware of, never been produced with the modified Pechini method. Malic acid and tartaric acid were therefore tested as complexing agents, and the calcination temperature was also varied. The goal was to achieve a single-phase nanocrystalline powder using a lower synthesis temperature than previously achieved by others with other synthesis methods.

Part II
Background

3 The properties of the relevant cations

3.1 Properties affecting complexing

The cations to be considered in this study are copper, aluminium, sodium, lanthanum, tungsten and molybdenum along with functional groups such as hydroxyl and carboxyl groups. As described in Section 1, two quite different oxides were studied and to understand the mechanisms which are influencing the synthesis of these, some theory has to be reviewed. The one of the most important aspects to understand is the cations ability to form stable complexes.

During complexation of cations in a solution, complexes are formed by a Lewis acid base reaction. By definition, a Lewis acid is an electron pair acceptor while a Lewis base is an electron pair donor [30]. Lewis acids and bases can be categorized as hard or soft [31]. Acids are identified empirically as hard or soft by measuring the opposite order of strengths of the complexes they form with halide ion bases. The strength is measured by the equilibrium constant for the formation of the complex, K_f. The strength of the complexes using hard acids will be in the order $I^- < Br^- < Cl^- < F^-$, while soft acids form complexes with strengths of the opposite order [30]. Thus, the binding strength of hard acid cations will increase with the electrostatic parameter ($\xi = z^2/r$, where z is the valence of the ions and r is the distance between two ions) of the anion, while the binding strength of soft acid cations will increase when the polarizability of the

anion increases. These two trends indicate that hard acid cations form complexes where ionic interactions are dominant, while soft acid cations form complexes where the covalent interactions are most important. Bases can also be classified as hard and soft in a similar way. Soft bases will have a low electronegativity and be easily polarized while hard bases will have a high elecronegativity and be hard to polarize. Halides and oxoanions will most often form complexes where ionic bonds will dominate and are therefore classified as hard bases. From the previous discussion it follows that hard acids tend to bind to hard bases in an ionic manner, while soft acids tend to bind to soft bases where covalent bonds dominate [31]. The properties of the acids and bases in these two categories can be summarized as in Table 3.1.

Table 3.1: *An overview of the properties of hard and soft acids and bases [31].*

	Acid	**Base**
Soft	Low positive charge	Low electronegativity
	Large size	Easily oxidized
	Highly polarizable	Highly polarizable
Hard	High positive charge	High electronegativity
	Small size	Hardly oxidized
	Hardly polarizable	Hardly polarizable

The described image is quite simple, but several other factors may also contribute to the energy of formation of the complexes. There may, for instance, be a competition between the solvent and the complexing agent if the reaction is happening in a solution, substituents of the acid or base would possibly need to be rearranged to permit the formation of the com-

plexes and steric repulsion between substituents on the acid and the base may affect the bonding [30]. The chemical hardness of the elements of interest in their relevant ionic form is summarized in Table 3.2 of each element in their relevant ionic form along with the relevant functional groups.

Table 3.2: *The chemical hardness of the relevant functional groups and ions of the elements chosen for this work.*

Ion	**Hardness of ion**
Cu^{2+}	Borderline
Cu^{+}	Soft
Al^{3+}	Hard
Na^{+}	Hard
La^{3+}	Hard
W^{6+}	Hard
Mo^{6+}	Hard
R-COO^{-}	Hard
R-OH	Hard

Many articles are describing a method called the Pechini method where one is taking advantage of the properties of complexed metal cations for making homogeneous powders. According the the work of Selbach *et al.* on making $BiFeO_3$ using the Pechini method [3], cations of borderline hardness will be complexed to a greater extent by hydroxyl groups (R-OH) compared to carboxyl (R-COO^{-}) groups. The same trend has also been indicated by Liu *et al.* [32]. The same result was also obtained during the preliminary master thesis work by the author [1], where the Pechini method was studied

for $CuAlO_2$ and $NaLa(WO_4)(MoO_4)$. This may indicate that the hydroxyl group is softer than the carboxyl group, thus complexing softer cations better.

3.2 Acidic, amphoteric and basic oxides

For understanding the mechanisms in the wet chemical synthesis of $CuAlO_2$ and $NaLa(WO_4)(MoO_4)$, it may be quite important to know how the individual elements behave as oxides. Oxides can act either as an acid or a base when dissolved in water. When an acidic oxide is dissolved in water, it will bind a H_2O molecule and release a proton to the solvent, making the solvent more acidic. A basic oxide will get a proton when dissolved in water, making the solvent more basic [30]. In general, the frontier part between the metallic and non-metallic elements in the periodic table, is characterized by amphoteric oxides, and the amphoterism changes with the oxidation state of the elements. These amphoteric oxides can behave as both acids and bases. Amphoterism is connected to a significant degree of covalent character in the bonds between the elements, either because the metal cation is strongly polarizing or it is polarized by the oxygen atom attached to it. The amphoterism thus reflects the metal cation's ability to polarize the oxide ions around it. Typically, the degree of amphoterism, and thus covalence, will increase when the oxidation number increases [30]. The acidity of the oxides of the relevant cations is presented in Table 3.3.

Table 3.3: *The acidity of the oxides of the relevant cations [30].*

Ion	**Acidity of oxide**
Cu^{2+}	Basic
Cu^{+}	Basic (more than Cu^{2+})
Al^{3+}	Amphoteric
Na^{+}	Basic
La^{3+}	Basic
W^{6+}	Mildly acidic
Mo^{6+}	Strongly acidic

4 Properties of the materials

4.1 Phases, structures and conductivity in the Cu-Al-O system

4.1.1 The phases in the Cu-Al-O system

An important challenge when producing $CuAlO_2$ is controlling the partial pressure of oxygen inside the gels. In the synthesis of $CuAlO_2$, both too low and too high partial pressures of oxygen will cause other phases to appear, as Figure 4.1 is presenting. The temperature is easier to control, but for obtaining $CuAlO_2$ a lower temperatures than possible in air, the partial pressure of oxygen needs to be controlled strictly.

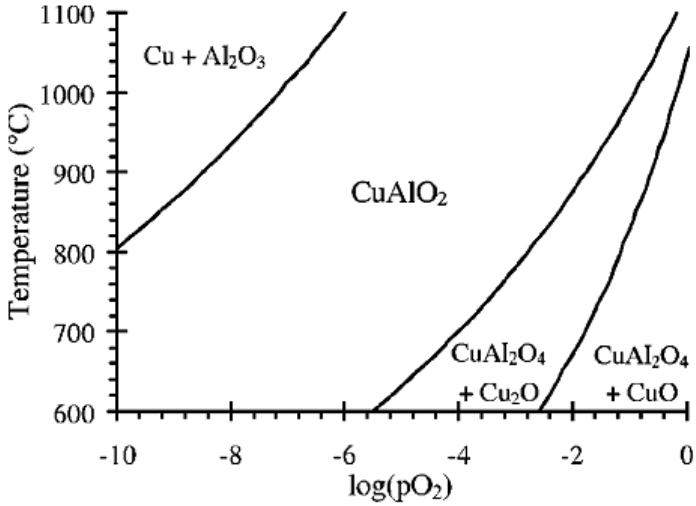

Figure 4.1: *The phase diagram for the Cu-Al-O system at 1 atm where the temperature versus the logarithm of the partial pressure of oxygen is presented [33].*

Several synthesis methods have been tested for making $CuAlO_2$ such as the hydrothermal metathesis reaction [15], the sol-gel synthesis using an alkoxide precursor solution [34, 35, 36], the solid state synthesis [37] and the Pechini method [4, 28, 29] where several parameters have been studied such as the type of precursors, calcination temperature and calcination atmosphere. In general it can be seen that a high temperature or reducing atmosphere, or both simultaneously, is required to get pure nanocrystalline $CuAlO_2$, and so far the lowest calcination temperature in air has been reported to be 1000 °C by Ghosh *et al.* by using copper acetate monohydrate and aluminium nitrate nonahydrate as precursors and citric acid as complexing agent and methanol as polymerization agent [29]. Ren *et al.* investigated the use of nitrogen atmosphere during calcination and found a calcination temperature of 900 °C for $CuAlO_2$ films made with the same

cation precursors as Ren *et al.* and acrylic acid (AA) as complexing agent and isopropyl alcohol (IPA) as polymerizing agent [28]. The molar ratio of Cu:Al:AA:IPA was 1:1:100:2.

Reaction equations for making $CuAlO_2$ have been proposed in many articles [28, 34, 38, 39]. First, CuO and Al_2O_3 are produced in air at temperatures below 600 °C before CuO and Al_2O_3 will react further to form spinel $CuAl_2O_4$ as described in Euquation 1 [28]:

$$CuO + Al_2O_3 \rightarrow CuAl_2O_4 \tag{1}$$

By further reaction between $CuAl_2O_4$ and CuO, $CuAlO_2$ can be formed by the reaction in Equation 2 [28]:

$$2\ CuAl_2O_4 + 2\ CuO \rightarrow 4\ CuAlO_2 + O_2 \tag{2}$$

These equations are driven to the right when the partial pressure of oxygen is reduced, giving a larger amount of $CuAlO_2$. According to the work of Jacob *et al.* [39], the equations above are all thermodynamically spontaneous at higher temperatures in air. According to the same work, there are two more ways of making $CuAlO_2$, but these are spontaneous for lower temperatures. The reactions are presented in Equation 3 and 4.

$$4\ Cu + O_2 + 2\ Al_2O_3 \rightarrow 4\ CuAlO_2 \tag{3}$$

$$Cu_2O + Al_2O_3 \rightarrow 2\ CuAlO_2 \tag{4}$$

The reaction in Equation 3 are driven to the right when the partial pressure of oxygen is increased while the reaction in Equation 4 should not

occur in too high partial pressures of oxygen, as $CuAl_2O_4$ may be produced instead.

4.1.2 The crystal structure and conductivity of $CuAlO_2$

The crystal structure of $CuAlO_2$ is called delafossite which is a hexagonal, layered crystal structure, as seen in Figure 4.2. Hexagonal layers of Cu^+ and layers of edge-shared AlO_6-octahedra are stacked alternately, perpendicular to the c axis, as indicated in Figure 4.2. No oxygen atoms are present within the Cu^+ layers, and only two oxygen atoms are linearly coordinated to each Cu^+ in axial positions [11, 40].

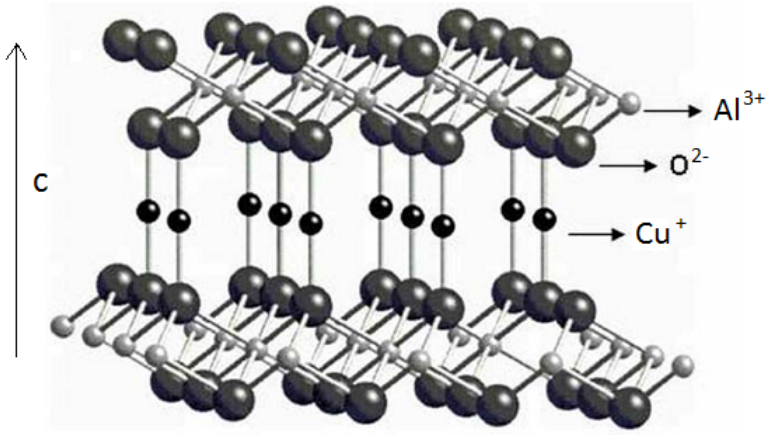

Figure 4.2: *Delafossite structure of $CuAlO_2$. The image is taken from Nagarajan et al. and has been slightly modified by the author [40].*

The p-type conduction in delafossite $CuAlO_2$ is due to holes in the Cu^+ layers [40]. The reported conductivity of $CuAlO_2$ films has been up to $6.7{\cdot}10^{-2}$ S cm^{-1} at room temperature for films made with sol-gel [28]

which is about the same as for single crystal $CuAlO_2$ measured for the plane perpendicular to the c-direction in Figure 4.2 [41]. Others have obtained values of 2.4 S cm^{-1} for anisotropically grown films using a technique of spinning on nanocrystals made hydrothermally [15], but this result has not been reproduced. For sintered pressed pellets with no intentional doping, a value of $7.7{\cdot}10^{-3}$ S cm^{-1} has been reported at room temperature for polycrystalline pellets of $CuAlO_2$ with the delafossite structure using a method using a nanoparticle based Cu(I)-acetate-loaded boehmite precursor [42].

The close-packed Cu^+ ions creates a semiconducting band perpendicular to the stacking direction owing to d-orbital holes and $Cu^+(d^{10})$–$Cu^+(d^{10})$ bonding [43, 44]. Based on the symmetry of the delafossite structure, the conduction in the Cu^+ close-packed planes would be much higher than for the Cu-O-Cu direction [43]. Conductivity measurements on $CuAlO_2$ laminar crystals by Lee *et al.* reveiled that the conductivity along the Cu^+ planes was at least 25 times higher than along the c-direction [44].

The phase Cu_2O in the phase diagram in Figure 4.1 is known to have good p-type properties and the local symmetries around Cu^+ and O^{2-} in this phase are similar to $CuAlO_2$, except that the nearest-neighbouring cations of the oxide ion are one Cu^+ and three Al^{3+} in the delafossite and not four Cu^+ [11]. The high p-type conductivity in Cu_2O is due to the higher coordination of Cu^+ to each O^{2-} in Cu_2O compared to $CuAlO_2$ making the conduction along the c-axis much higher than for $CuAlO_2$. For the same reason, it is considered that the mixing and interactions between the 3d-orbitals of Cu^+ and 2p-orbitals of O^{2-} in Cu_2O are greater than those in $CuAlO_2$ which leads to larger dispersion of the valance band in Cu_2O compared to $CuAlO_2$. This results in larger mobility and narrower band gap (2 eV) in comparison with that of $CuAlO_2$. As a consequence,

$CuAlO_2$ has a larger band gap than Cu_2O which gives rise to optical transparency [45].

The phase $CuAl_2O_4$ is known to be an insulator and would thus degrade the electrical conductivity of $CuAlO_2$ if present as impurity [46]. CuO would, on the other hand, increase the p-type conductivity in $CuAlO_2$ if present [47].

4.2 Structure and luminescence of $NaLa(WO_4)(MoO_4)$:Eu

4.2.1 The crystal structure of $NaLa(WO_4)(MoO_4)$

The complex oxide $NaLa(WO_4)(MoO_4)$ will adopt a scheelite-like structure with the general formula AA'XX'O_8 where A = Li^+, Na^+, K^+, Rb^+ or Cs^+; A' = Y^{3+}, La^{3+} or Gd^{3+}(rare earths); and X = Mo^{6+} and X' = W^{6+} [26, 27, 48]. The general scheelite structure with the formula AXO_4 can be viewed in Figure 4.3. Both tungsten oxides and molybdenum oxides adopt a scheelite structure with both alkali metals and rare earths disordered in the same site and the similar ionic radii of tetrahedral Mo^{6+} (41 pm) and W^{6+} (42 pm) [49] which makes it possible to prepare solid solutions of the type AA'$(WO_4)_{2-x}(MoO_4)_x$. In this structure, Mo^{6+} and W^{6+} are coordinated by four oxygen atoms in a tetrahedral site, and the rare-earth/alkali site is eight coordinated, with two sets of rare earth-oxygen distances.

A few research groups have been able to make single-phase nanocrystalline Eu-doped $NaLa(WO_4)(MoO_4)$. Lu *et al.* obtained pure Eu-doped $NaLa(WO_4)(MoO_4)$ using Eu_2O_3, La_2O_3, HNO_3, $NaNO_3$, $H_{40}N_{10}O_{41}W_{12}$ and $(NH_4)_6Mo_7O_{24}{\cdot}4H_2O$ as raw materials with $CO(NH_2)_2$ as a fuel and a calcination temperature of 900 ^{o}C [27]. The doping concentration varied

between 4 and 14 %. Similar materials have been successfully made, for instance by Neeraj *et al.* who obtained single-phase Eu-doped $NaLn(WO_4)_{2-x}(MoO_4)_x$, where Ln = Y, Gd, using solid state synthesis at a temperature of 800 ºC for 60 hours [26]. Li *et al.* made $NaLa(MoO_4)_2$ doped with Eu^{3+} and Tb^{3+} using the hydrothermal synthesis route [50] and by Wang *et al.* using the solid state method at 800 ºC [51] . The Pechini method was successfully employed using citric acid as complexing agent by Guo *et al.* to make Eu-doped $NaLa_5(MoO_4)_4$ with a calcination temperature as low as 550 ºC [52]. Gu *et al.* managed to obtain uniform Eu^{3+} and Tb^{3+} doped $NaLa(WO_4)_2$ nanocrystals solvothermally [53]. Compounds like $NaEu_{0.96}Sm_{0.04}(MoO_4)_2$ have been obtained by using the Pechini method using a calcination temperature of 700 ºC [54].

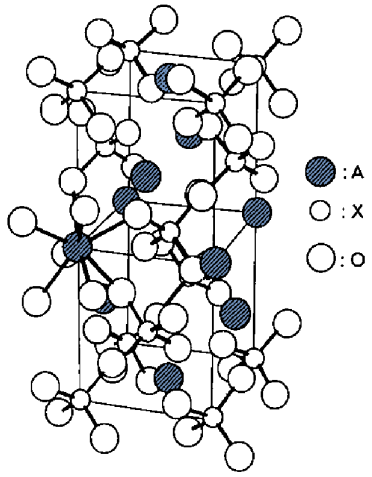

Figure 4.3: *The scheelite structure with the A -cations represented as large blue circles, the X-cations by small white circles and the large white circles represent the O atoms [55].*

4.2.2 Doping and luminescence of $NaLa(WO_4)(MoO_4)$

Doping with Eu^{3+} will substitute the lanthanide-cation in the scheelite structure [26] giving rise to a luminescent character [27, 56]. Transitions of pure trivalent rare earth ions are parity forbidden transitions. Due to the Laporte parity rule [55] dipole transitions can only occur between energy levels with an angular momentum parameter (J) differing by one. The notation for these energy states is $^{2S+1}L_J$, where the exalted number is called the multiplisity and is given by 2S+1 where S is the total spin angular momentum and J is the total angular momentum of the electrons in the filling orbital [5].

The Laporte parity rule implies that dipole transitions within the 4f level (with the same parity) are dipole-forbidden. But previous studies have showed that when Eu^{3+} is placed in a non-centrosymmetric position in the lattice, such as in the scheelite structure, the luminescent character will be enhanced [57, 58]. Once the Eu^{3+} ion is included as dopant into non-centrosymmetric sites in a host lattice, the internal electric and magnetic fields of the host can break certain symmetries resulting in a mixing of states with different parity giving rise to weakly allowed transitions. These weakly allowed transitions give rise to long lifetimes (in the order of µs to ms) of the energy levels of the trivalent rare earth ions [59]. Some transitions, e.g. those where $\Delta J = 0, \pm 2$, are hypersensitive to this effect and become dominant in the spectrum even for small deviations from centrosymmetry [55]. This is the reason for the strong appearance of the $^5D_0 \rightarrow {}^7F_2$ transition line when Eu^{3+} is substituting for La^{3+} in $NaLa(WO_4)(MoO_4)$. A spin-forbidden transition thus gives rise to phosphorescence, which is a slower transition compared to fluorescence and the lifetime of this transition is in the order of 230 μs [60]. Figure 4.4 is presenting the various energy states

for the $4f$-electrons in Eu^{3+} and a list combining the different transitions with their unique emission wavelengths is given in Table 4.1.

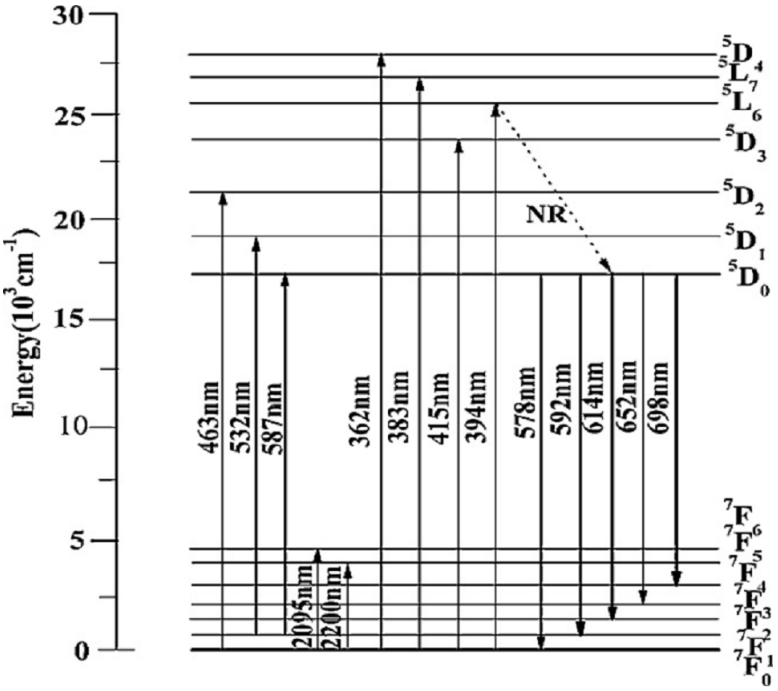

Figure 4.4: *Energy levels for $4f^n$ configurations of trivalent Eu^{3+} with some calculated excitation and emission energies [60].*

Table 4.1: *The unique emission wavelengths of different transitions in Eu^{3+} at room temperature [61].*

Optical transition	Wavelength (nm)
$^5D_1 \rightarrow {}^7F_0$	526
$^5D_1 \rightarrow {}^7F_1$	536
$^5D_1 \rightarrow {}^7F_2$	555, 557.5
$^5D_0 \rightarrow {}^7F_0$	578
$^5D_0 \rightarrow {}^7F_1$	590.3, 592, 593.5
$^5D_0 \rightarrow {}^7F_2$	614.4, 616.4, 618.2
$^5D_0 \rightarrow {}^7F_3$	649, 652
$^5D_0 \rightarrow {}^7F_4$	687, 691.5, 694.5, 697, 700.5

Excitation of Eu^{3+} occurs for preferred wavelengths as presented in Table 4.2. These are normally detected by using the strongest emission wavelength, i.e. from the $^5D_0 \rightarrow {}^7F_2$ transition.

Table 4.2: *The unique excitation wavelengths of different transitions in Eu^{3+} at room temperature [61].*

Optical transition	Wavelength (nm)
$^7F_0 \rightarrow {}^5D_4$	362
$^7F_1 \rightarrow {}^5D_4$	367
$^7F_0 \rightarrow {}^5G_4$	375.5
$^7F_0 \rightarrow {}^5G_2$	381
$^7F_1 \rightarrow {}^5L_7$	386
$^7F_0 \rightarrow {}^5L_6$	395
$^7F_1 \rightarrow {}^5L_6$	400
$^7F_0 \rightarrow {}^5D_3$	416.5
$^7F_0 \rightarrow {}^5D_2$	465
$^7F_1 \rightarrow {}^5D_2$	473

5 The synthesis method

5.1 The Pechini method - the polymerizable complex method

The Pechini method is inspired by the well-known sol-gel method. In the sol-gel synthesis a stable solution (the sol) containing the relevant cations as metal alkoxides is transformed into a gel by hydrolysis and condensation reactions [6]. The cations will thus be an integrated part of the gel network. The main advantage of forming a gel is the ability to get a more

homogeneous distribution of the cations. If the cations are not able to form such suitable metal alkoxides, the Pechini method can be used [5, 6].

The fundamental idea behind the Pechini method is to reduce the individual behavior of each cation by complexation before immobilizing them in a gel [62]. If the complexation of the cations is sufficient and the gel is stable, this can reduce the formation of secondary phases during the evaporation and decomposition process at high temperatures. The reaction chemistry behind the gelling process includes a condensation reaction between a carboxylic acid and an alcohol, i.e. an esterification [6]. The carboxylic acid and the alcohol should both have more than one functional group, making it possible for the same molecule to participate in esterification reactions more than once (i.e. polyesterification) and make a network. This network is called a gel. The most common carboxylic acid and polyalcohol when using this method is citric acid and ethylene glycol. The citric acid will act as the complexing agent in this system in addition to being part of the polyesterification with ethylene glycol, forming the gel network. Therefore, the cations will not be an integrated part of the network when employing the Pechini method, but only weakly bonded to the gel, immobilizing the cations into certain positions. An example reaction between ethylene glycol and citric acid is shown in Figure 5.1. Using this method, a lower synthesis temperature may be obtained compared to other methods.

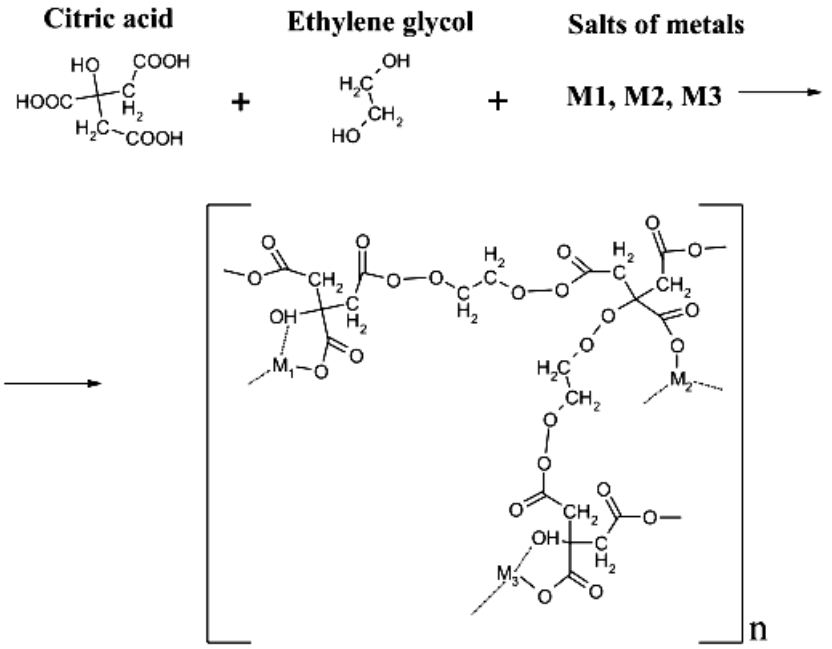

Figure 5.1: *Polyesterification reaction between citric acid and ethylene glycol encapsulating the metal cations [63].*

Many carboxylic acids tend to form stable complexes with a variety of metal cations over a fairly wide range of pH, allowing for the relatively easy synthesis of oxides of considerable complexity, with a high degree of homogeneity and small particle sizes [6]. Malonic, malic and tartaric acid are fairly similiar to citric acid, which has three carboxyl groups and one hydroxyl group. Malonic acid has the fewest number of such groups having only two carboxyl groups as seen in Figure 5.2a. Malic acid has a longer carbon chain than malonic acid, and one hydroxyl group in addition to the two carboxyl groups, see Figure 5.2b. Tartaric acid is the compound with the highest number of functional groups of these three, resembling

citric acid the most, having both two carboxyl and two hydroxyl groups, as in Figure 5.2c. This would ideally make tartaric acid able to form a gel network without the addition of EG. Both malic and tartaric acid has two forms of isomers.

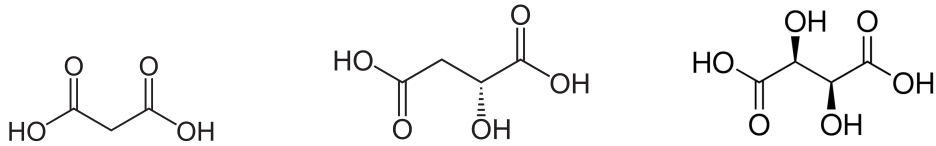

Figure 5.2: *a) Malonic acid [64], b) D-malic acid [65] and c) D-tartaric acid [66].*

The main disadvantage for the Pechini method lies in the lack of control over particle size, shape, and morphology. Only during calcination can the size be modified in a controlled fashion. In traditional sol-gel, the metal cations become an integral part of the gel network, but in the Pechini method, these are only held in place by weaker complexing bonds [6]. Due to this, the Pechini method is not suitable for producing specific structures such as two-dimensional chains and ribbons. The particles obtained after calcination are almost always spherical or nearly spherical, and some aggregation from sintering should be expected. At least 300 °C is needed to make a powder free from organic contaminants and some complexing agents require an even higher temperature [6].

According to several studies [67, 68], nucleation before sufficient immobilization of the cations may also occur if the concentration of the cations are too high. This may cause problems with unwanted secondary phases. When the cation concentration is lower, it takes a longer time to reach supersaturation and nucleation followed by precipitation can thus be avoided.

5.2 Varying the parameters during the synthesis

5.2.1 Amount of complexing and polymerization agents

The primary purpose of the complexing agent and polymerization agent is to immobilize the cations in a gel, but these additives also have a secondary effect. During the last stages of gelling, a smoldering reaction may occur, and these additives will then act as fuels for this reaction. The synthesis method would then be more similar to the *Low temperature combustion synthesis method* described by Zhang [69]. The same reactions would continue during the calcination. The amount of complexing and polymerization agent would determine how reducing the environment inside the gel is, affecting the final product according to the phase diagram in Figure 4.1. Grain growth seems to be enhanced when the temperature of the combustion or smoldering reaction is increased [69]. According to the work of Zhao *et al.* on nanostructured $Li_2Fe_xSiO_4/C$ with Fe [70], more starch in the sol would result in more residual carbon in the N_2-calcined gels. This carbon would give a more reducing internal atmosphere in the gels in the same way as increased amounts of complexing agents and polymerization agents in the gels in this work. Based on this, stoichiometric amounts of complexing and polymerization agents could be estimated by reaction equations. Equation 5, which is created by the author and supervisor of this work, gives a stoichiometric reaction equation for creating $CuAlO_2$ in nitrogen atmosphere where one mole each of the precursor materials copper acetate and aluminium nitrate are mixed with one mole of ethylene glycol per one mole of copper acetate or aluminium nitrate along with α moles of complexing

agent for producing no left-over carbon.

$$\begin{array}{c} \mathrm{Cu(C_2H_3O_2)_2 + Al(NO_3)_3 + C_2H_6O_2 + \alpha \cdot compl.agent} \\ \Downarrow \\ \mathrm{CuAlO_2 + \beta{\cdot}CO + \frac{3}{2} + N_2 + \gamma \cdot H_2O + \delta{\cdot}C} \end{array} \tag{5}$$

By inserting the molecular formula for the complexing agents into this equation and balancing it would give the α-values 1, 0.5 and 1 for malonic acid, malic acid and tartaric acid, respectively. Tartaric acid has enough hydroxyl groups to be able to form a gel without the help of ethylene glycol and the α-value for tartaric acid when no ethylene glycol is present, is 4. But this reaction equation is highly ideal and would not be very likely to occur exactly in a real gel as parts of the reaction would occur during the gelling in air, making this reaction only a tool for adjusting the concentration of complexing agent. In theory, one should go lower in concentration than this equation is predicting when calcining in N_2-atmosphere as excess carbon would be produced for higher values, making the reduction to elemental copper more likely. When the calcination is taking place in air, the concentration should be higher than the anticipated value, as more reducing conditions are needed to obtain the correct phase.

Compared to the solid state method, Ghosh *et al.* found that the production of $CuAlO_2$ with the Pechini method would give smaller particles due to the presence of the complexing agent, citric acid [29].

5.2.2 The temperature and atmosphere in the gels during synthesis

An overview of the relationship between temperature, partial pressure of oxygen and phases present for the Cu-Al-O system was presented in the phase diagram in Figure 4.1. During the wet chemical synthesis of the oxide, as described in Section 5.1, a relatively large amount of material has to be burned off during smoldering and calcination to create a pure oxide. During a smoldering reaction local areas of the gel may reach relatively high temperatures causing the reduction of the gel to be even more prominent. Many reactions could happen to create more oxidizing or reducing atmospheres compared to the external atmosphere. The evolving nitrous and carbonaceous gases would expel the oxygen in the gels, creating a more reducing atmosphere, moving towards the left in the phase diagram in Figure 4.1. The reducing environment along with elevated temperatures will result in a lower oxidation state for the cations which are able to change their oxidation state [33]. Li *et al.* have studied the effect of different cation precursors on the purity and calcination temperature of $CuAlO_2$ microcrystallites when using the Pechini method with citric acid as complexing agent [4]. They showed that a calcination temperature of 1050 °C is needed to get microcrystallites of $CuAlO_2$ in air when using the Pechini method, but if the calcination is done in reducing atmosphere, e.g. N_2, a lower temperature can be achieved.

5.2.3 Other parameters

Deng *et al.* have made p-type $CuAlO_2$ with the delafossite structure by employing the Pechini method using the nitrate-citrate route [36], and showed

that mechanical milling is necessary for obtaining pure $CuAlO_2$ using short annealing periods.

The choice of precursors is also important as they will cause the reducing conditions in the gel during smoldering to be different. Ghosh *et al.* found that when using nitrate-precursors in the Pechini method, a lower calcination temperature could be obtained [29].

Other parameters would be harder to control, such as how much the viscosity of the gels affects the stirring, making the conditions in the gel very different in parts of the gel. Slight differences in the temperature of the hot-plates may also cause self-ignition at different stages during gelling and the temperature of the smoldering reaction could be very different as different amounts of fuel could be present and they may burn with different temperatures. The additives in the gel may play an important role to how easily the gel self-ignites and thus the temperature inside the gels could therefore be very different. Different solubilities of the carboxylic acids would also affect the amounts possible to add to the gels. The larger the size of the carboxlic acids, the lower solubility they have in solution [71]. If the gel was to assemble quickly into a lump, inhomogeneous conditions would not be avoidable as only some parts would be in direct contact with the hot-plate. Different amounts of gel in the crucibles during calcination may also affect the calcination results.

Part III
Experimental

6 The synthesis of $CuAlO_2$

A complete overview of the syntheses of the $CuAlO_2$ gels can be seen in Table 6.1. The metal cation precursors used for the synthesis of these gels were $Cu(CH_3COO)_2 \cdot H_2O$ (98 %, trace metal basis, Sigma Aldrich) and $Al(NO_3)_3 \cdot 9\ H_2O$ ($\geq$ 98 %, Sigma Aldrich). The precursors were dissolved in distilled water aiming for a concentration of 0.25 mol/l for the Cu-precursor and 0.6 mol/l for the Al-precursor. The exact concentration of the solutions was determined by standardization as described in Appendix A. The carboxylic acids used as complexing agents were malic acid (99.0 %, Sigma Aldrich), tartaric acid (99.0 %, Sigma Aldrich) and malonic acid (99.0 %, Merck Schuchardt). To match the synthesis desciption given by Selbach *et al.* for the production of $BiFeO_3$ [3], 0.02 moles of each of the carboxylic acids were dissolved individually in 20 ml of distilled water in different beakers. The gels following this recipe are hereby called batch 1. Some gels were made with 1.5 and 2 times this amount of complexing agent, called batch 2. The solutions in batch 4 were made with concentrations equal to or lower than the α-values from Equation 5 in Section 5.2.1, and were made as an attempt to enhance a stoichiometric reaction equation giving $CuAlO_2$ when calcined in nitrogen atmosphere. The dissolved carboxylic acids were placed on hot-plates with a magnetic stirrer, heating them to 50 ^{o}C. Then 0.01 moles of each of the dissolved metal cation precursors were added to each beaker with complexing agent and water, the Cu-precursor first. To obtain as good complexation of the metal cations as

possible, the pouring was done quite slowly. At last, 0.02 moles of ethylene glycol (EG) (100 %, VWR) as a polymerizing agent were added to the syntheses in batch 1. Half of this amount of EG was added to the malic acid complexed solutions of batch 2 to enhance the polymerization and to the solutions in batch 4. Some gels were added 15 and 30 times more ethylene glycol compared to the amount in batch 1, based on the recipe of Li *et al.* on $CuAlO_2$ [4] and these syntheses are hereby called batch 3.

After addition of all the chemicals into each beaker, the temperature in the beakers was raised to 100 ºC on hot-plates for batch 1 and 4 to make the solutions boil and finally self-ignite. This self-ignintion was attemped to be avoided for batch 2 and 3, using a hot-plate temperature of only 80 ºC. The gels were left on the hot-plates for a few minutes after ended gelling and self-ignition to make them more dry. Batch 3 had to be dried in a drying cabinet at 120 ºC for 20 hours. The cooled dry gels were then ground to homogeneous powders in agate mortars. The ground powders from batch 1 were calcined in alumina crucibles in air for 6 hours at 1000 and 1150 ºC in addition to 500 ºC for 1 hour. Data for the calcination temperatures 600 and 900 ºC were collected from a previous work by the author [1]. Batch 2 and 3 were calcined in alumina crucibles in air for 1 hour at 600, 900, 1000 and 1150 ºC. The powders from batch 4 were calcined in alumina crucibles in nitrogen atmosphere for 1 hour at 600, 800 and 1000 ºC. The heating and cooling rates were 200 ºC per hour for all the samples. The furnaces used for the calcinations were Nabertherm P330 and Nabertherm B180 and gave comparable results for the same temperatures. Each calcination was performed on approximately 0.2 to 1.5 grams of gel and varied with the densities of the uncalcined gels and the amount of additives left in them after the smoldering reactions.

Table 6.1: *An overview of the syntheses of $CuAlO_2$. The complexing and polymerizing agent is listed for each sample. The notation "CA" means the target material $CuAlO_2$, while "mn", "m" and "t" refers to malonic, malic and tartaric acid, respectively. The number in each cell is representing the number of moles of the substance per mole of one type of cation in each synthesis. The name given for each batch is stating the main difference of the batches.*

Batch	Label	Complexing agent	EG
	CA-2mn	Malonic (2)	0
	CA-2mn-2EG	Malonic (2)	2
1	CA-2m	Malic (2)	0
standard recipe	CA-2m-2EG	Malic (2)	2
	CA-2t	Tartaric (2)	0
	CA-2t-2EG	Tartaric (2)	2
	CA-3m-1EG	Malic (3)	1
2	CA-4m-1EG	Malic (4)	1
more complexing	CA-3t	Tartaric (3)	0
agent	CA-4t	Tartaric (4)	0
	CA-2m-15EG	Malic (2)	15
3	CA-2m-30EG	Malic (2)	30
more EG	CA-2t-15EG	Tartaric (2)	15
	CA-2t-30EG	Tartaric (2)	30
	CA-0.5mn-1EG	Malonic (0.5)	1
	CA-0.75mn-1EG	Malonic (0.75)	1
	CA-1mn-1EG	Malonic (1)	1
4	CA-0.25m-1EG	Malic (0.25)	1
stoichiometric	CA-0.5m-1EG	Malic (0.5)	1
in nitrogen	CA-0.75m-1EG	Malic (0.75)	1
	CA-0.5t-1EG	Tartaric (0.5)	1
	CA-0.75t-1EG	Tartaric (0.75)	1
	CA-1t-1EG	Tartaric (1)	1

7 The synthesis of $NaLa(WO_4)(MoO_4)$:Eu

The gels for making $NaLa(WO_4)(MoO_4)$ were synthesized during a previous study by the author [1]. A flow scheme of the synthesis route can be seen in Figure 7.1. The precursors for making the $NaLa(WO_4)(MoO_4)$ gels were $NaNO_3$ ($\geq$ 99.0 %, Sigma Aldrich), $La(NO_3)_3 \cdot 6\ H_2O$ (99.9 %, trace metal basis, Sigma Aldrich), H_2WO_4 (99.0 %, Sigma Aldrich) and $(NH_4)_6Mo_7O_{24} \cdot 4\ H_2O$ (99.98 %, trace metal basis, Sigma Aldrich). The $NaNO_3$(s) was dried at 200 ºC for 24 hours before usage, while the La- and Mo-precursors were dissolved in water before each solution was complexed individually by malic and tartaric acid before they were included in the syntheses. The correct concentrations of the complexed solutions were determined by standardization, as described in Appendix A, and the values are presented in Table 7.1. The molar ratio between the metal cations and complexing agent was 1:1. A route developed by Gil *et al.* [2] was used as a basis when complexing the W-cations. Previously, this route had been successful using citric acid as the complexing agent. The tungstic acid was first dissolved in a diluted solution of ammonium hydroxide (25 %, VWR) and then kept at 80 ºC for 24 hours on a magnetic stirrer. When the solution became clear, the carboxylic acid (malic or tartaric acid) was slowly added to get a 1:1 ratio between the cations and complexing agent, and the stirring was then continued for 24 hours at 80 ºC under a lid.

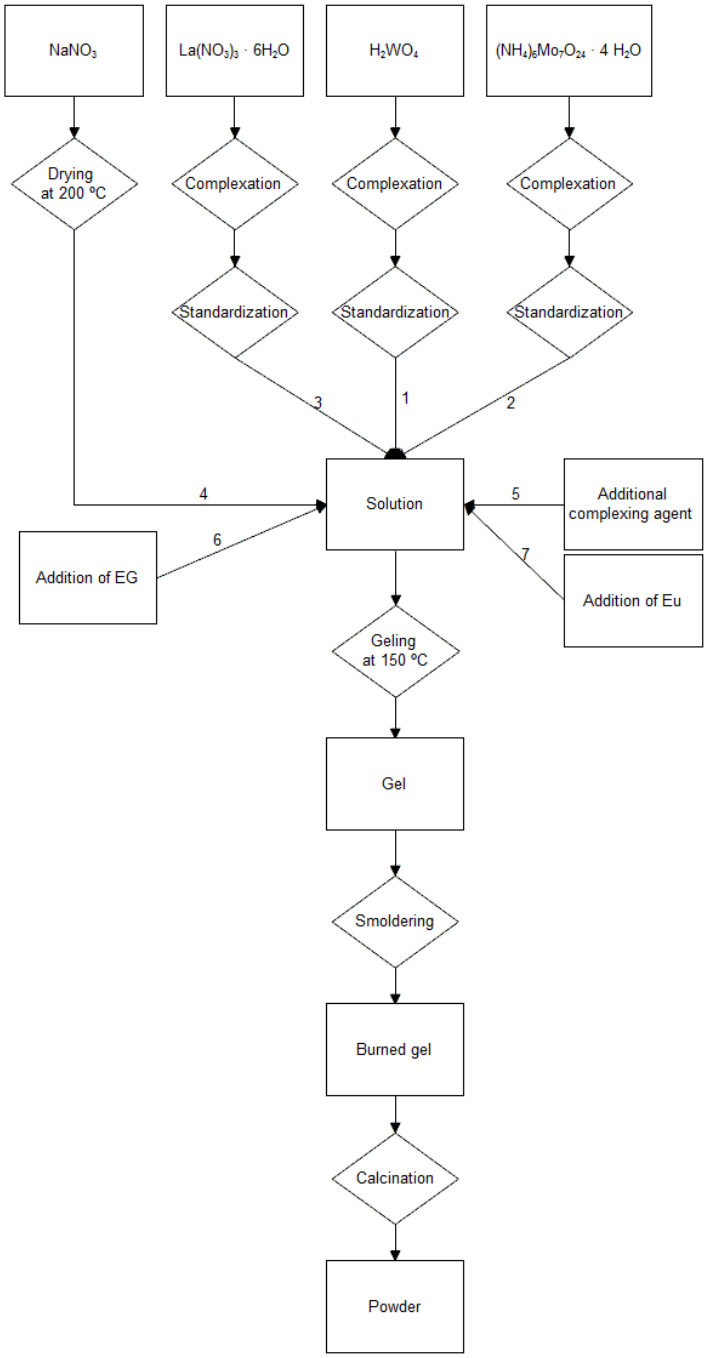

Figure 7.1: *Flow chart of synthesis route of Eu-doped $NaLa(WO_4)(MoO_4)$. The numbered arrows are indicating the order of additions [1].*

Table 7.1: *The concentration of the complexed cation solutions for the syntheses of Eu-doped $NaLa(WO_4)(MoO_4)$ determined by standardization [1].*

Cation	**Complexing agent**	**Concentration of cation [mmol/g]**
W^{6+}	Malic acid	0.2527
W^{6+}	Tartaric acid	0.2221
Mo^{6+}	Malic acid	0.0567
Mo^{6+}	Tartaric acid	0.0637
La^{3+}	Malic acid	0.3086
La^{3+}	Tartaric acid	0.3033

An overview of the syntheses is shown in Table 7.2. From the complexed cation solutions, 0.01 moles of tungsten and molybdenum were added to each beaker while 0.0096 moles of sodium and lanthanum were added to give room for 0.0008 moles of europium. The precursors were added in the order tungsten, molybdenum and then lanthanum. At last the dried Na-precursor was added along with an additional amount of complexing agent to give a ratio between Na and complexing agent of 1:1. $Eu(NO_3)_3 \cdot 6\ H_2O$ (99.9 %, trace metal basis, Sigma Aldrich) was added to each beaker before 0.04 moles of ethylene glycol (100 %, VWR) were added to some of the syntheses. The solutions were heated to 100 ºC on hot-plates and as the water content became critically low, the gels self-ignited initiating smoldering reactions. The gels were left on the hot-plates for a few additional minutes to dry. The cool and dry gels were crushed into homogeneous powders in agate mortars before they were calcined in alumina crucibles in air at 300, 400, 500, 600 and 1000 ºC (Nabertherm B180). Previous work by the author [1] is presenting values for a calcination temperature of 700 ºC.

Table 7.2: *An overview of the syntheses of Eu-doped $NaLa(WO_4)(MoO_4)$. The complexing agent and polymerizing agent are listed for each synthesis. The label "NLMW" is referring to the first letter of every cation in the target material, while "m" and "t" means malic and tartaric acid, respectively. The number in each cell is representing the number of moles of the substance per mole of one type of cation in each synthesis.*

Label	**Complexing agent**	**Polymer. agent**
NLMW-m	Malic (4)	0
NLMW-mEG	Malic (4)	4
NLMW-t	Tartaric (4)	0
NLMW-tEG	Tartaric (4)	4

8 The characterization of the materials

All of the ground gels and the calcined powders of both materials were analysed with X-ray diffraction (XRD) using a Bruker AXS D8 Focus. The diffractograms were analysed using a software made by Bruker AXS called Diffrac.EVA version 2.1. The phases and the approximated phase ratios were found using this software. XRD can only detect crystalline phases, and the percentages given on composition does not say anything about the amorphous phases in the samples. The calculations of crystallite sizes in the samples were also done using this software, applying the most intense reflection of the phase which did not overlap with another reflection. The Scherrer equation [72], with the integral breadth approximation and a shape factor of 0.9, was utilized. Values of mass loss were also found by weighing the samples before and after calcination. Secondary electron

scanning electron microscopy (SE-SEM) was performed in a Zeiss Ultra 55 (field emission gun) and Zeiss Supra 55 VP (field emission gun) for obtaining images of a selection of the powder samples.

The electrical conductivity of batch 2 and 3 of $CuAlO_2$ calcined at 1150 ºC, were measured with a standard multimeter and the method is further described in Appendix B. For this purpose, 10 mm pellets with 0.5-1 mm thickness were pressed at 0,8 tons of pressure and sintered at 1350 ºC for 2 hours. As the amount of powder for each sample was quite small, all the powders calcined at 1150 ºC for each batch were blended in agate mortars and then pressed into pellets. Silver contacts were painted on the pellets. The density of the sintered pellets was measured with Arkimedes' method as described in Appendix C. The cross-section of these pellets were imaged in a TM3000 tabletop SEM using the back scattered electron signal.

The photoluminescence emission was studied for Eu-doped $NaLa(WO_4)(MoO_4)$ on 11 mm pellets pressed at 8 tons, with a Leica DM5500 B using an excitation wavelength of 405 nm. The excitation properties were measured using a setup from Horiba Jobin Yvon IBH which included a FluoroCube photon-counting spectrometer detecting the emission intensity at 615 nm. Fourier Transform Infrared (FT-IR) spectroscopy was used on one gel and its calcination products using a Bruker IFS 66v. The powders (0.5 mass%) were added to KBr which was dried at 120 ºC in a vacuum cabinet for 24 hours. Pellets of 11 mm were pressed at 8 tons of pressure. The data were plotted with Opus viewer 6.5 from Bruker Optik GmbH. The surface area of the 700 ºC calcined samples of $NaLa(WO_4)(MoO_4)$, produced during an earlier work by the author [1], was measured with a TriStar 3000 V6.05 A, and calculated by using the BET-isotherm [73].

Part IV
Results

9 The characterization of $CuAlO_2$

9.1 Observations during the syntheses

During the last stages of the gelling of batch 1 (standard recipe), the final volume of the gels were increased with lower amounts of added complexing and polymerizing groups, e.g. the volume of the gels was in the order CA-2mn > CA-2mn-2EG > CA-2m > CA-2m-2EG > CA-2t > CA-2t-2EG. Smoldering reactions could be spotted all the gels most intense for the malonic acid complexed gels. This resulted in a dark color for all the gels in this batch, as seen in Figure 9.1. None of the gels of batch 2 (more complexing agent) self-igninted during the gelling but stayed in the pre-set temperature range of 80 ^{o}C. White precipitations could be observed for the tartaric acid complexed solutions in this batch and these occurred before the visible formation of the gel network. This resulted in a more pale color of the dry gels compared to the gels with malic acid, as seen in Figure 9.1. In batch 3 (more EG), the sample CA-2m-15EG self-ignited exceeding temperatures of 110 ^{o}C. These gels were hard to dry on the hot-plates and needed to be dried in a drying cabinet. Hard blue to turquoise crystals were produced in the bottom of the crucibles during calcination, insoluble both in water and ethanol. Smoldering reactions probably took place in the other gels in this batch as well, as the color of the dry gels were darker for all the gels compared to the gels in batch 2, as seen in Figure 9.1.

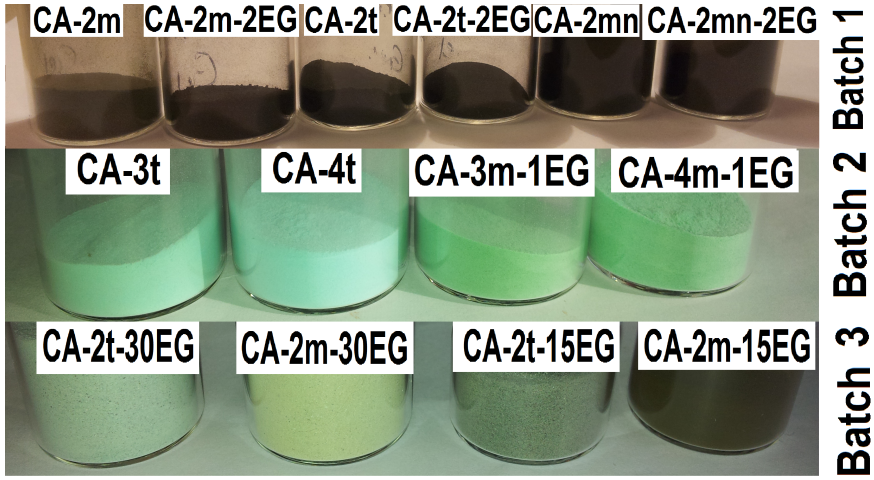

Figure 9.1: *The color of the dry gels of batch 1 (standard recipe), 2 (morecomplexing agent) and 3 (more EG) before calcination.*

The gels in batch 4 (stoichiometric in nitrogen) were quite similar in appearance to the gels of batch 1. The malonic acid complexed gels experienced the most vigorous reactions compared to all the samples in this work with increasing speeds and temperatures for increasing amounts of malonic acid. The sample CA-1mn-1EG burned fast with a bright color and the termometer showed 190 ºC before it was crushed by the intense heat. The volume of these gels shows the same effect as seen for the gel volumes in batch 1, as the CA-1mn-1EG gel seemed to have the largest volume of the gels in batch 4. The malonic acid complexed gels of batch 4 evolved laminar layers of different colors during the calcinations at 600 and 800 ºC. The sample CA-0.5mn-1EG was brown on the top, brown red in the middle and grey at the bottom, CA-0.75mn-1EG was dark brown on the top and brown red at the bottom and CA-1mn-1EG was green on the top, dark brown in the middle, then red and finally yellow at the bottom.

9.2 Phases present and crystallite sizes in the gels and calcined gels

9.2.1 Batch 1 (standard recipe)

The XRD spectra of the gels in batch 1 are presented in Figure 9.2, while Table 9.1 is presenting the percentage of the present phases calculated from these diffractograms.

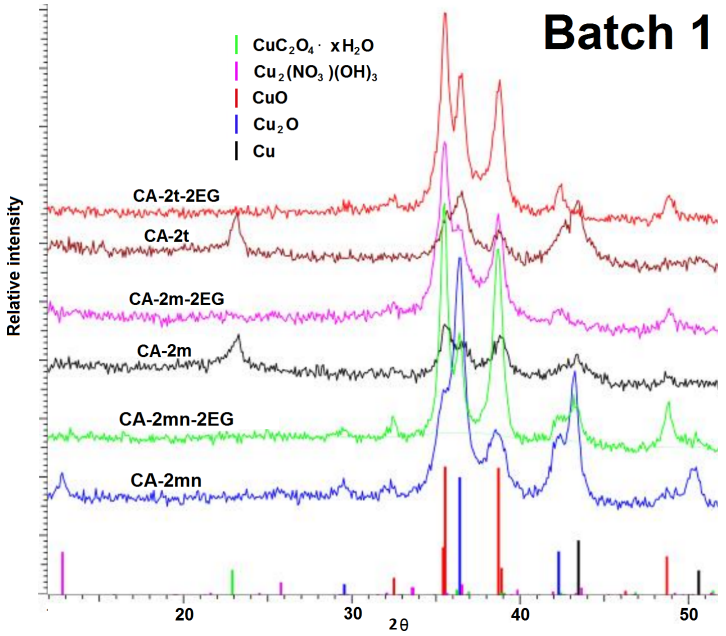

Figure 9.2: *XRD spectra of the uncalcined gels of batch 1.*

Salts with divalent copper were found generally in the gels without EG. The gels with EG were showing lower amounts of elemental copper and higher amounts of CuO. The gels labeled with a star (*) visibly self-ignited

during gelling, but as described in Section 9.1, the other gels in this batch experienced smoldering reactions as well.

Table 9.1: *An overview of the present phases in the gels of $CuAlO_2$ from batch 1. The numbers are representing the contribution in mass percentage for each crystalline phase. The gels labeled with a star (*) visibly self-ignited during the gelling.*

Gel	**$CuC_2O_4 \cdot x\ H_2O$**	**$Cu_2(NO_3)(OH)_3$**	**CuO**	**Cu_2O**	**Cu**
CA-2mn*		3	27	68	2
CA-2mn-2EG*			67	32	1
CA-2m	34		58	5	3
CA-2m-2EG			93	7	
CA-2t	20		28	47	5
CA-2t-2EG			56	44	

The diffractograms for sample CA-2m calcined at temperatures 500, 600 [1], 900 [1], 1000 and 1150 ºC is presented in Figure 9.3. The diffractograms are showing the general trends for the samples in batch 1. The gels of batch 1 were calcined at 500 ºC, giving pure CuO for all the gels with crystallite sizes of about 10 nm for all the gels. Calcination during the preliminary master thesis [1] at 600 ºC resulted in CuO with crystallite sizes of about 15 nm for all the gels in batch 1 except for the gel with tartaric acid and EG as this powder also contained traces of $CuAl_2O_4$.

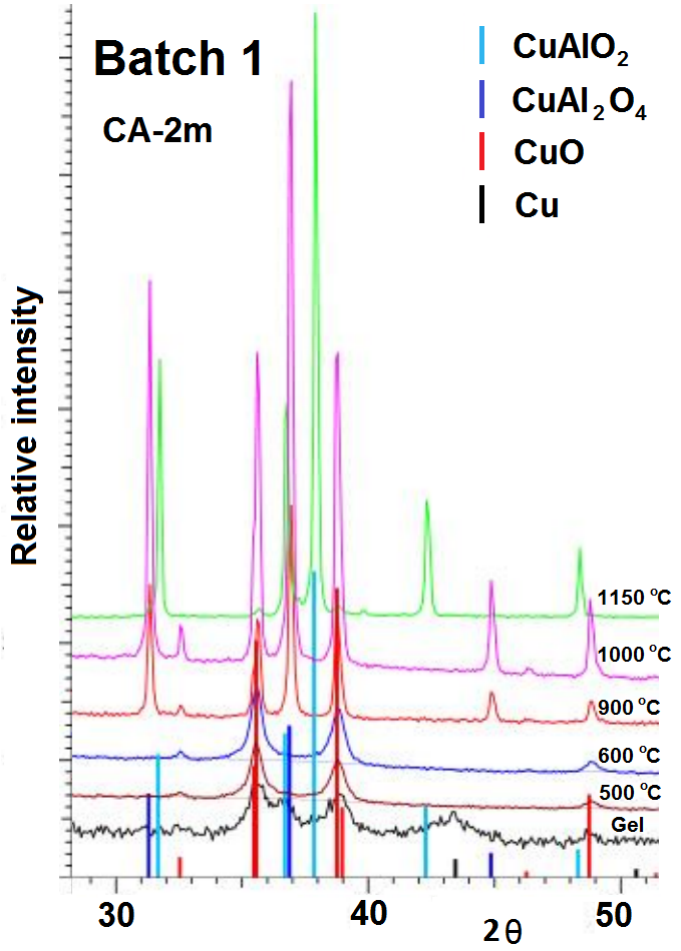

Figure 9.3: *XRD spectra for CA-2m uncalcined and calcined at various temperatures representing the general trends in batch 1.*

The approximated mass percentages of each phase in the calcined gels are presented in Table 9.2 and are calculated from the XRD spectra of the samples. Calcination at 900 °C in air was done during previous work by the

Table 9.2: *The phase composition of the gels in batch 1 calcined at various temperatures. The samples calcined at 500 °C are not included as they only contained CuO. The numbers are indicating the approximated mass percentage of each crystalline phase calculated from the XRD spectra of the samples.*

Gel	600 ºC [1]	900 ºC [1]	1000 ºC	1150 ºC
CA-2mn	CuO	$CuAl_2O_4$+CuO	$CuAl_2O_4$+CuO	$CuAlO_2$+$CuAl_2O_4$+CuO
		61+39	**66+34**	**82+16+2**
CA-2mn-2EG	CuO	$CuAl_2O_4$+CuO	$CuAl_2O_4$+CuO	$CuAlO_2$+$CuAl_2O_4$+CuO
		62+38	**64+36**	**89+9+1**
CA-2m	CuO	$CuAl_2O_4$+CuO	$CuAl_2O_4$+CuO	$CuAlO_2$+$CuAl_2O_4$+CuO
		62+38	**64+36**	**75+23+2**
CA-2m-2EG	CuO	$CuAl_2O_4$+CuO	$CuAl_2O_4$+CuO	$CuAlO_2$+$CuAl_2O_4$+CuO
		64+36	**63+37**	**84+14+2**
CA-2t	CuO	$CuAl_2O_4$+CuO	$CuAl_2O_4$+CuO	$CuAlO_2$+$CuAl_2O_4$+CuO
		63+37	**64+36**	**88+10+2**
CA-2t-2EG	CuO +$CuAl_2O_4$	$CuAl_2O_4$+CuO	$CuAl_2O_4$+CuO	$CuAlO_2$+$CuAl_2O_4$+CuO
	93+7	**63+37**	**65+35**	**90+8+2**

author [1] and showed an increase in the amount of $CuAl_2O_4$ (about 30 nm crystallite size) for all the gels in addition to the CuO phase. The $CuAl_2O_4$ phase was dominating for all the gels with about 63 mass% $CuAl_2O_4$ and 37 mass% CuO. Calcination at 1000 ºC confirmed this trend as the ratio now became approximately 65 mass% $CuAl_2O_4$ (about 40 nm crystallite size) and 35 mass% CuO (about 30 nm crystallite size) in all the gels in batch 1.

The calcination in air at 1150 ºC resulted in a dominating $CuAlO_2$ phase for all the samples. The percentage of $CuAlO_2$ was between 75-90 mass% for all the samples with a trend of slightly more $CuAlO_2$ when EG was added. The crystallite size of the $CuAlO_2$ was 40-50 nm for all the samples. Impurity phases were present in all the samples and were mostly $CuAl_2O_4$ and CuO. Sample CA-2t-2EG had the highest percentage of $CuAlO_2$ for a calcination temperature of 1150 ºC. Weak reflections at 37.2 and 39.8 º were seen in the XRD spectra for all the samples calcined at 1150 ºC. These reflections are due to traces of the hexagonal $CuAlO_2$ phase with a P63/mmc spacegroup.

9.2.2 Batch 2 (more complexing agent)

In the uncalcined gels CA-3t and CA-4t of batch 2, some reflections as shown in Figure 9.4, could not be identified, more unknown reflections could be seen for the gels with tartaric acid without EG. Also, more precipitation of tartaric acid could be seen with increasing concentration of complexing agent for the samples CA-3t and CA-4t. Copper oxalate hydrate could be seen in all the four gels and no elemental copper could be seen. The mass

percentage of each crystalline phase in the uncalcined gels is presented in Table 9.3.

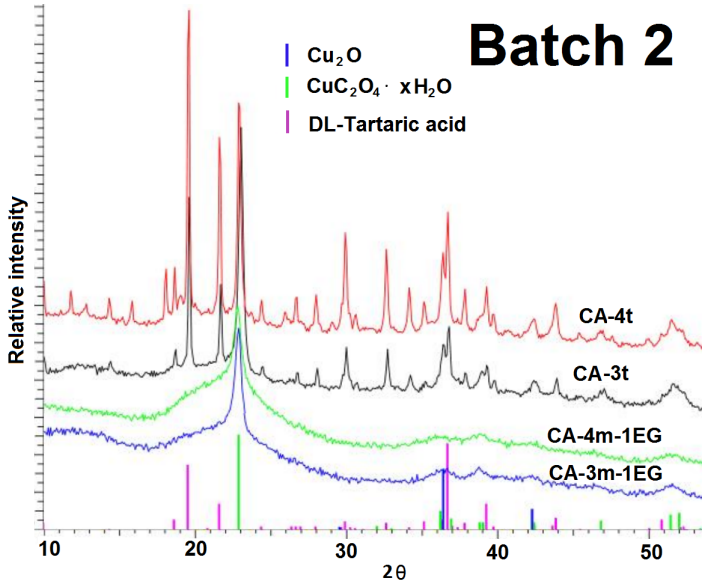

Figure 9.4: *XRD spectra of the gels in batch 2. Several unidentified reflections are seen for the tartaric acid complexed gels.*

Table 9.3: *An overview of the present phases in the gels of $CuAlO_2$ from batch 2. The numbers are representing the contribution in mass percentage for each crystalline phase.*

Gel	Tartaric acid	$CuC_2O_4 \cdot x\ H_2O$	Cu_2O
CA-3m-1EG		92	8
CA-4m-1EG		99	1
CA-3t	36	62	2
CA-4t	48	50	2

The 600 ºC calcined gels of batch 2 all contained $CuAl_2O_4$ and CuO, both with crystallite sizes of about 20 nm. The calcined gels complexed with tartaric acid contained traces of $CuAl_2O_4$ but for the malic acid complexed gels, the $CuAl_2O_4$ could be found in slightly larger amounts (4 and 7 mass% for CA-3m-1EG and CA-4m-1EG, respectively). Figure 9.5 is presenting the XRD spectra of sample CA-4m-1EG and CA-4t calcined at 600, 900, 1000 and 1150 ºC and Table 9.4 is summarizing the calculated ratios between the phases in each sample which are calculated from the XRD spectra. There are only small differences in the calcined samples when comparing the different gels although the uncalcined gels have quite different composition. The calcinations at 900 and 1000 ºC in air resulted in $CuAl_2O_4$ with about 30 and 40 nm crystallite sizes at 900 and 1000 ºC, respectively and CuO with about 25 and 30 nm at 900 and 1000ºC, respectively. The ratio between these two phases was about the same as for batch 1. Calcination in air at 1150 ºC gave about 85 mass% $CuAlO_2$ with $CuAl_2O_4$ and CuO as impurities. The crystallite sizes of the $CuAlO_2$ phase were in the range 35-45 nm for all the gels. More complexing agent seemed to give a small reduction of the crystallite size in the order of a few nanometers.

Reflections in the XRD spectra at 37.2 and 39.8 º were seen for all the calcined sample at 1150 ºC in this batch indicating traces of hexagonal $CuAlO_2$ with the P63/mmc space group.

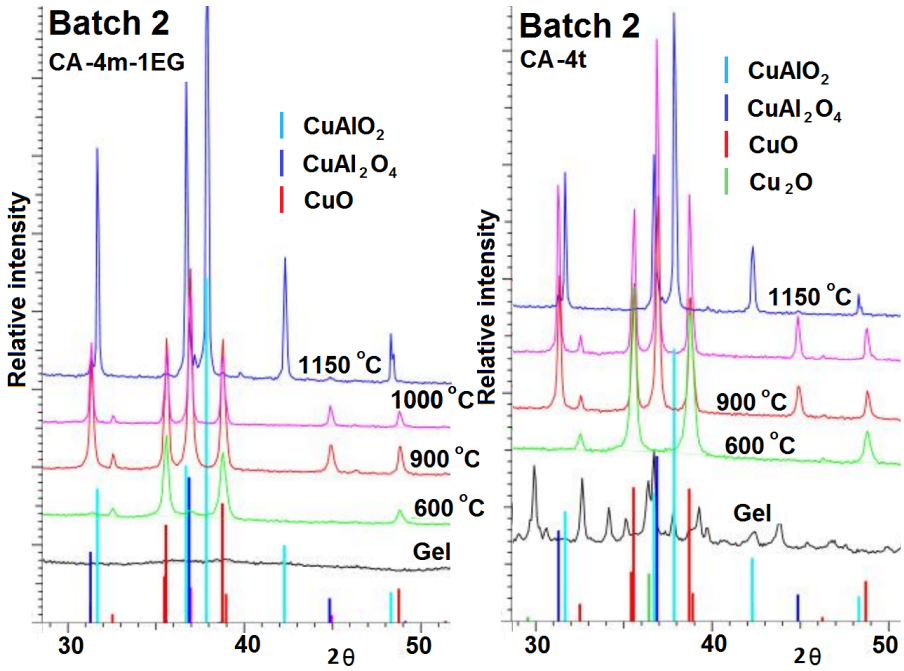

Figure 9.5: *XRD spectra of the samples CA-4m-1EG and CA-4t from batch 2, uncalcined and calcined at various temperatures representing the general trends of batch 2.*

Table 9.4: *The phase composition of the gels in batch 2 calcined at various temperatures. The numbers are indicating the approximated mass percentage of each crystalline phase calculated from the XRD spectra of the samples.*

Gel	600 ºC	900 ºC	1000 ºC	1150 ºC
CA-3m-1EG	$CuO+CuAl_2O_4$	$CuAl_2O_4+CuO$	$CuAl_2O_4+CuO$	$CuAlO_2+CuAl_2O_4+CuO$
	96+4	**57+42**	**66+34**	**83+16+1**
CA-4m-1EG	$CuO+CuAl_2O_4$	$CuAl_2O_4+CuO$	$CuAl_2O_4+CuO$	$CuAlO_2+CuAl_2O_4+CuO$
	93+7	**58+42**	**65+35**	**84+15+1**
CA-3t	$CuO+CuAl_2O_4$	$CuAl_2O_4+CuO$	$CuAl_2O_4+CuO$	$CuAlO_2+CuAl_2O_4+CuO$
	99+1	**58+42**	**65+35**	**85+14+1**
CA-4t	$CuO+CuAl_2O_4$	$CuAl_2O_4+CuO$	$CuAl_2O_4+CuO$	$CuAlO_2+CuAl_2O_4+CuO$
	99+1	**59+41**	**66+34**	**87+12+1**

9.2.3 Batch 3 (more EG)

As seen in Figure 9.6, the gels CA-2t-30EG, CA-2t-15EG and CA-2m-30EG in batch 3 were quite similar with a fairly equal distribution of copper oxalate hydrate and elemental copper. The malic acid complexed gel with a smaller addition of EG evolved quite differently. The one complexed with malic acid consisted mainly of mono- and divalent copper oxide and only 2 percentages of elemental copper. The mass percentages of each crystalline phase in the uncalcined gels are presented in Table 9.5. The gels marked with a star (*) visibly self-ignited during gelling, but as described in Section 9.1, the other gels in this batch probably experienced smoldering reactions as well.

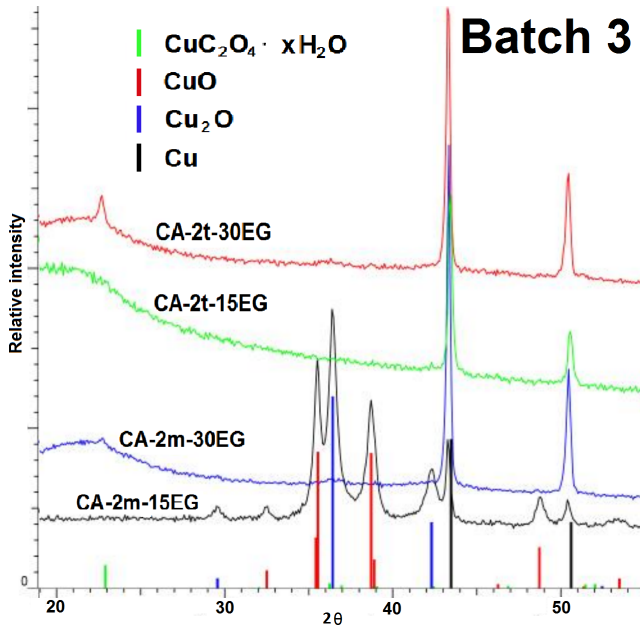

Figure 9.6: *XRD spectra of the gels in batch 3.*

Table 9.5: *An overview of the present phases in the gels of $CuAlO_2$ from batch 3. The numbers are representing the mass percentage for each crystalline phase. The gel marked with a star (*) visibly self-ignited during gelling.*

Gel	$CuC_2O_4 \cdot x\ H_2O$	CuO	Cu_2O	Cu
CA-2m-15EG*		83	15	2
CA-2m-30EG	49		2	49
CA-2t-15EG	49			51
CA-2t-30EG	66		1	33

The 600 ºC calcined powders of batch 3 consisted mostly of CuO with crystallite sizes of 13-20 nm, except for CA-2t-30EG which also had about 3 mass% of Cu_2O. Figure 9.7 shows the diffractograms for the samples CA-2m-15EG and CA-2m-30EG both uncalcined and calcined at 600, 900, 1000 and 1150 ºC in air. The mass percentages of the crystalline phases in the samples, calculated from the XRD spectra, are summarized in Table 9.6. Even though the gels are quite different, the calcined samples are quite similar.

After calcination at 900 ºC in air, the powders consisted of $CuAl_2O_4$ and CuO both with crystallite sizes of about 25 nm, with $CuAl_2O_4$ as the dominant phase. More EG in the gels gave 53-55 mass% of $CuAl_2O_4$ and about 60 mass% of $CuAl_2O_4$ for the gels with less EG. A slight increase in the amount of $CuAl_2O_4$ could be seen for the calcined gels with malic acid. At 1000 ºC, these differences disappeared and the composition became approximately 65 mass% $CuAl_2O_4$ and 35 % CuO for all the gels. The crystallite sizes increased to about 35-40 nm for $CuAl_2O_4$ and 27 nm for CuO.

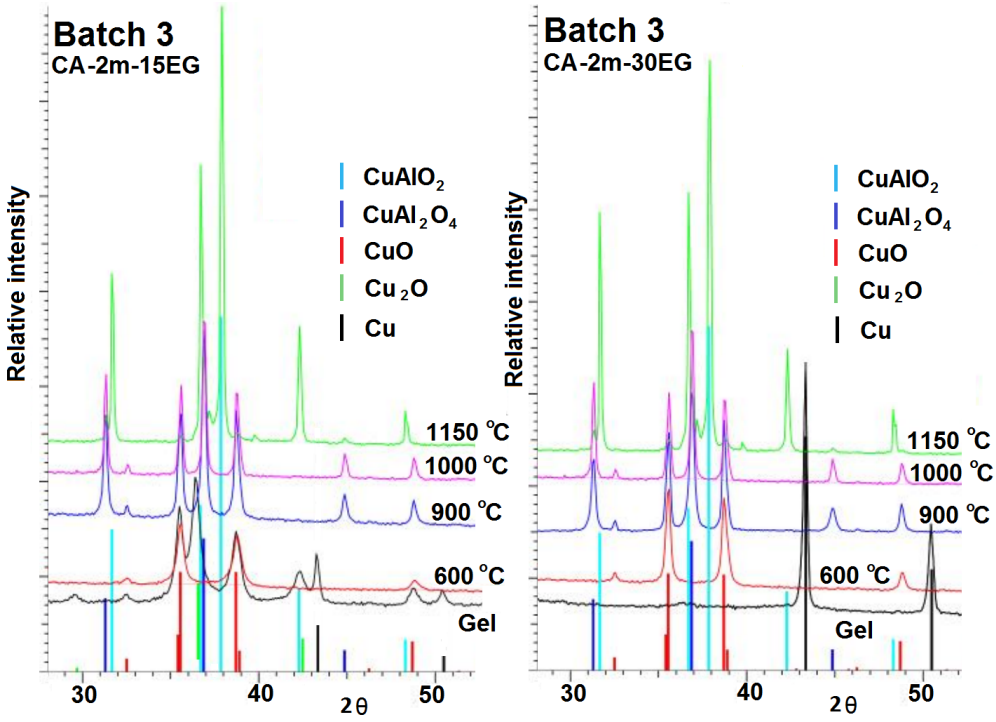

Figure 9.7: *XRD spectra of the samples CA-2m-15EG and CA-2m-30EG of batch 3, uncalcined and calcined at various temperatures representing the general trend of batch 3.*

Calcination at 1150 ºC in air resulted in varying amounts of $CuAlO_2$ with about 80-84 mass% for the gels with most EG, 72 mass% for CA-2t-15EG and 91 mass% for CA-2m-15EG, the last one being the highest mass percentage of $CuAlO_2$ obtained of all the samples in this work. The crystallite sizes were 35-40 nm for the $CuAlO_2$ phase. Malic acid seemed to give a slightly higher crystallite size compared to tartaric acid. The remaining part of the calcined gels calcined at this temperature was $CuAl_2O_4$ and CuO. Weak reflections at 37.2 º and 39.8 º were seen in the XRD spectra

Table 9.6: *The phase composition of the gels in batch 3 calcined at various temperatures. The numbers are indicating the approximated mass percentage of each crystalline phase calculated from the XRD spectra of the samples.*

Gel	600 ºC	900 ºC	1000 ºC	1150 ºC
CA-2m-15EG	CuO	$CuAl_2O_4$+CuO	$CuAl_2O_4$+CuO	$CuAlO_2$+$CuAl_2O_4$+CuO
		61+39	**65+35**	**91+8+1**
CA-2m-30EG	CuO	$CuAl_2O_4$+CuO	$CuAl_2O_4$+CuO	$CuAlO_2$+$CuAl_2O_4$+CuO
		55+45	**64+36**	**80+17+3**
CA-2t-15EG	CuO	$CuAl_2O_4$+CuO	$CuAl_2O_4$+CuO	$CuAlO_2$+$CuAl_2O_4$+CuO
		60+40	**65+35**	**72+26+2**
CA-2t-30EG	CuO+Cu_2O	$CuAl_2O_4$+CuO	$CuAl_2O_4$+CuO	$CuAlO_2$+$CuAl_2O_4$+CuO
	97+3	**53+47**	**65+35**	**84+15+1**

for all the samples calcined at 1150 ºC. These reflections are due to traces of the hexagonal $CuAlO_2$ phase with a P63/mmc spacegroup.

9.2.4 Batch 4 (stoichiometric in nitrogen)

As seen in Figure 9.8, all the gels in batch 4 contained significant amounts of both CuO and Cu_2O with quite low concentrations of elemental copper. Traces of γ-Al_2O_3 could be found in CA-1mn-1EG. This sample turned out to have the most vigourous smoldering reaction during the gelling, as described in Section 9.1. The mass percentages of each crystalline phase in the uncalcined gels are presented in Table 9.7. The gels marked with a star (*) visibly self-ignited during gelling.

In batch 4, the gels calcined at 600 ºC in nitrogen mostly contained nanocrystalline copper in the size range of 10-25 nm except for the calcined gels complexed with malonic acid which also contained significant amounts of Cu_2O. The sample CA-1mn-1EG also had traces of γ-Al_2O_3 with a cubic spinel structure [74].

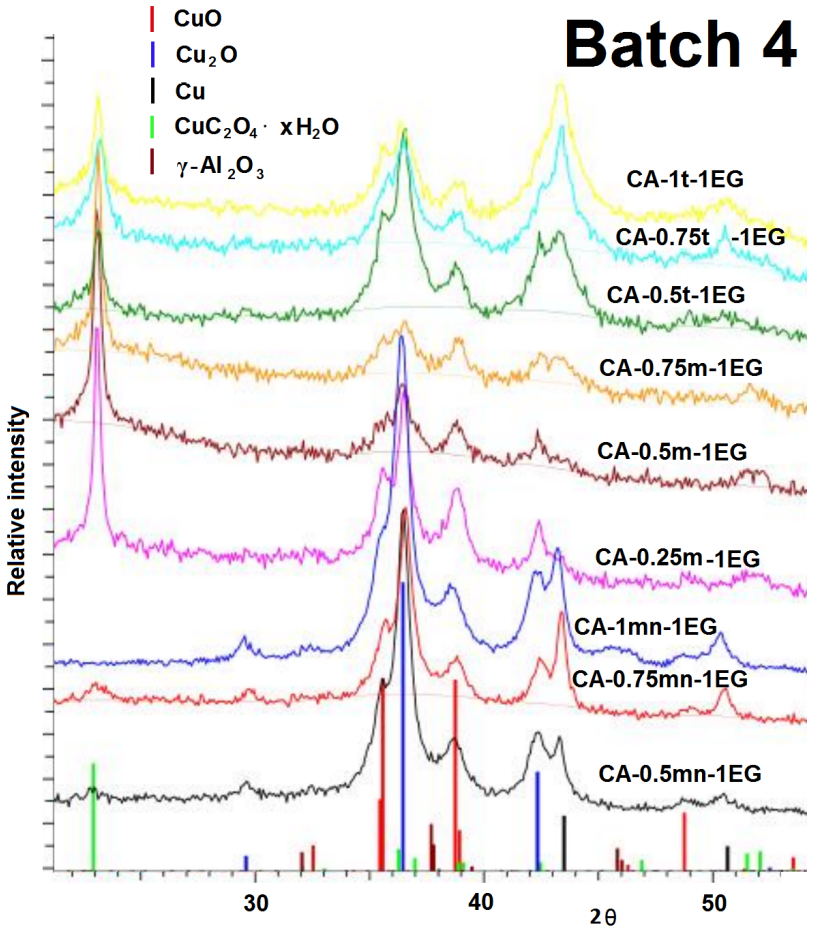

Figure 9.8: *XRD spectra of the uncalcined gels of batch 4.*

Table 9.7: *An overview of the present phases in the gels of $CuAlO_2$ from batch 4. The numbers are representing the contribution in mass percentage for each crystalline phase. Gels marked with (*) self-ignited during gelling.*

Gel	**γ-Al_2O_3**	**$CuC_2O_4 \cdot xH_2O$**	**CuO**	**Cu_2O**	**Cu**
CA-0.5mn-1EG*		18	59	21	2
CA-0.75mn-1EG*		24	52	17	7
CA-1mn-1EG*	12		62	22	3
CA-0.25m-1EG		50	40	9	1
CA-0.5m-1EG		75	19	5	1
CA-0.75m-1EG		50	22	27	1
CA-0.5t-1EG		34	49	13	4
CA-0.75t-1EG		28	22	45	5
CA-1t-1EG		45	38	8	9

After calcination at 800 ºC in nitrogen, the samples mostly contained nanocrystalline copper in the size range of 15-30 nm and small amounts of γ-Al_2O_3. The exception was the sample CA-0.5mn-1EG which contained about 20 mass% of $CuAlO_2$ and a few traces of Cu_2O in addition to copper and γ-Al_2O_3. The XRD spectra of this gel calcined at 600, 800 and 1000 ºC are presented in Figure 9.9 and shows the general trend for all the gels in this batch, except for a few differences. The gels calcined at 1000 ºC in nitrogen all contained nanocrystalline Cu with crystallite size of 20-30 nm, Cu_2O and Al_2O_3. All the samples calcined at 1000 ºC had the γ-Al_2O_3 except for the samples CA-1t-1EG, CA-0.5mn-1EG and CA-0.75mn-1EG which had the corundum phase instead.

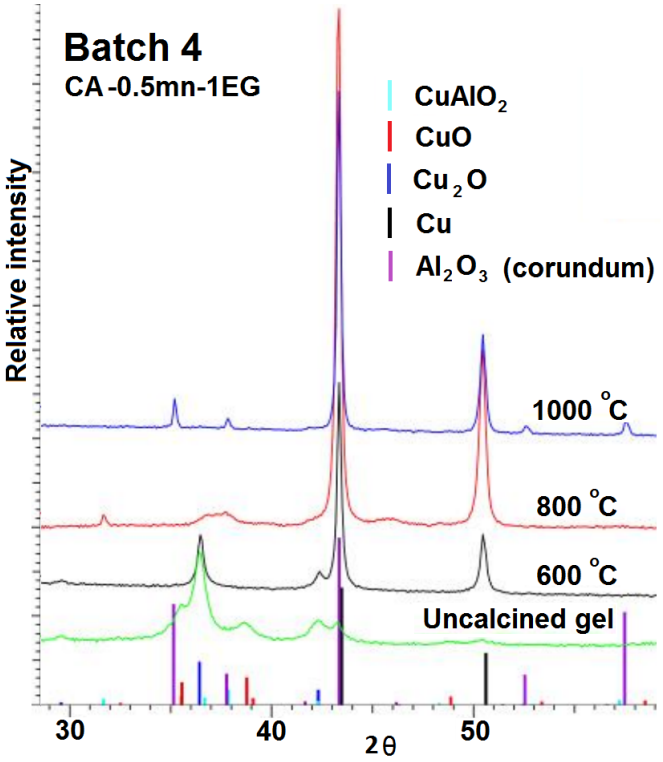

Figure 9.9: *XRD spectra of CA-0.5mn-1EG uncalcined and calcined at various temperatures.*

9.3 Loss of mass during calcination

The mass loss during the calcinations was calculated for each gel, and Table 9.8 presents the values for the remaining mass of the calcined gels of batch 1 (standard recipe).

Table 9.8: *The remaining mass in percentage after calcination in air at various temperatures for the gels in batch 1. The gels marked with a star (*) visibly self-ignited during the gelling.*

Gel	500 ºC	1000 ºC	1150 ºC
CA-2mn*	98	93	88
CA-2mn-2EG*	91	89	84
CA-2m	64	63	61
CA-2m-2EG	83	83	81
CA-2t	60	62	59
CA-2t-2EG	81	80	77

The gels that visibly self-ignited during gelling, marked with a star (*), have the highest percentage of remaining mass as there was a smaller amount of material left to be burned off during calcination. The same trend can be seen for batch 3 (more EG) which is presented in Table 9.10. The values for batch 2 are given in Table 9.9 and gives a low remaining mass percentage since none of the the gels self-ignited.

Table 9.9: *The remaining mass in percentage after calcination in air at various temperatures for the gels in batch 2.*

Gel	600 ºC	900 ºC	1000 ºC	1150 ºC
CA-3m-1EG	29	28	28	26
CA-4m-1EG	24	23	23	22
CA-3t	28	27	27	25
CA-4t	20	20	20	19

Table 9.10: *The remaining mass in percentage after calcination in air at various temperatures for the gels in batch 3. The gels marked with a star (*) visibly self-ignited during the gelling.*

Gel	600 ºC	900 ºC	1000 ºC	1150 ºC
CA-2m-15EG*	87	86	84	81
CA-2m-30EG	27	27	26	26
CA-2t-15EG	27	27	27	25
CA-2t-30EG	26	26	26	24

The trend seen in batches 1 and 3 when comparing the remaining percentage of mass after calcination with the visible self-ignition during gelling was not as clear in batch 4 (stoichiometric in nitrogen) as the variations in amount of complexing agent added for the samples would affect the mass loss, as seen in Table 9.11.

Table 9.11: *The remaining mass in percentage after calcination in nitrogen at various temperatures for the gels in batch 4. The gels marked with a star (*) visibly self-ignited during the gelling.*

Gel	600 ºC	800 ºC	1000 ºC
CA-0.5mn-1EG*	60	60	58
CA-0.75mn-1EG*	53	52	51
CA-1mn-1EG*	56	56	53
CA-0.25m-1EG	66	66	63
CA-0.5m-1EG	62	63	60
CA-0.75m-1EG	60	60	57
CA-0.5t-1EG	85	83	83
CA-0.75t-1EG	74	74	73
CA-1t-1EG	92	90	91

9.4 Particle size and morphology

The sample CA-2m of batch 1 (standard recipe), both uncalcined and calcined at 1150 ^{o}C was imaged with SEM as shown in Figure 9.10. Nanosized particles could be found in both of the samples. The particle size for the CA-2m sample about 15-20 nm. The samples CA-2mn and CA-2t calcined at 1150 ^{o}C were also imaged with SEM and images of the grain structure in the three samples are presented in Figure 9.11.

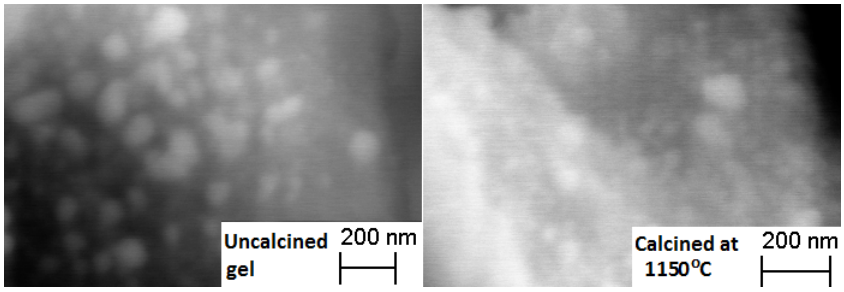

Figure 9.10: *SEM images of sample CA-2m from batch 1, uncalcined and calcined at 1150 ^{o}C.*

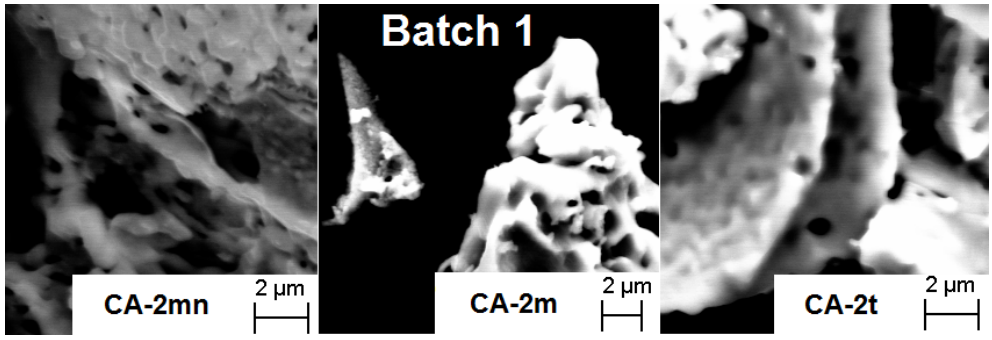

Figure 9.11: *SEM images of CA-2mn, CA-2m and CA-2t from batch 1 calcined at 1150 ^{o}C.*

The samples CA-3m-1EG and CA-3t calcined at 1150 ºC from batch 2 (more complexing agent) were imaged and the structures are quite similar for these two samples. The particles seemed to be larger in this batch compared to batch 1.

The images of the samples CA-2m-30EG and CA-2t-30EG of batch 3 (more EG) calcined at 1150 ºC are presented in Figure 9.13. The particles seem to be smaller for the malic acid complexed sample with sizes of about 100 nm, while the tartaric acid complexed sample had particles of about 200 nm. This is larger compared to batch 1.

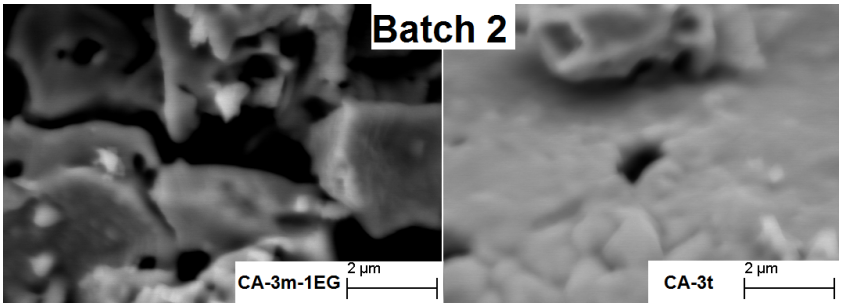

Figure 9.12: *SEM images of the samples CA-3m-1EG and CA-3t calcined at 1150 ºC.*

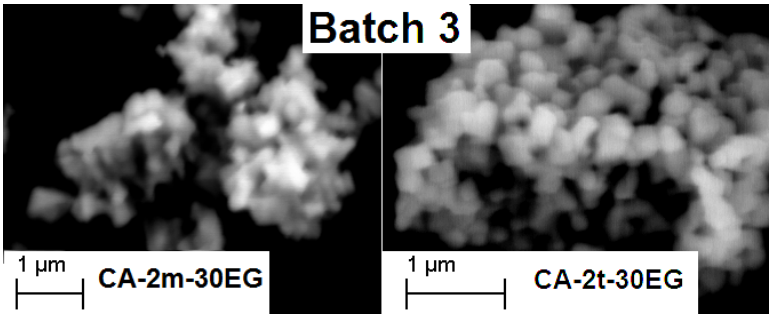

Figure 9.13: *SEM images of CA-2m-30EG and CA-2t-30EG from batch 3 calcined at 1150 ºC.*

9.5 Electrical conductivity

As described in Section 6, all the powders calcined at 1150 ºC were mixed for each batch before being pressed into pellets and sintered at 1350 ºC. All the pellets for both batch 2 (more complexing agent) and 3 (more EG) had high contact resistance between the silver paint contacts and the surface of the pellets. This made it hard to pass current through them and simple resistance measurements were therefore performed using a simple multimeter. The lowest resistance measured with this method was 1.62 kΩ for batch 2 and 81.3 kΩ for batch 3. Given the dimensions of the pellet and the contacts as described in Appendix B, assuming ideal conditions where a current would go in straight lines between the contacts, the resistivity of the pellets would be $3.1{\cdot}10^{-3}$ S cm^{-1} for batch 2 and $1.0{\cdot}10^{-4}$ S cm^{-1} for batch 3 when choosing the smallest measured value for each batch. Table 9.12 presents the calculated conductivities.

Table 9.12: *The calculated conductivities between the current contacts and voltage contacts of the pellets. The values denoted with the letters l and s are between the long contacts and short contacts, respectively. Three pellets were successfully made for batch 2 and two pellets were made for batch 3. All the values are given in S/cm.*

	Conductivity (S/cm)	
Pellet no.	**Batch 2**	**Batch 3**
1	$3.03{\cdot}10^{-5}{}_{l}$	$1.03{\cdot}10^{-4}{}_{l}$
	$7.66{\cdot}10^{-6}{}_{s}$	$6.76{\cdot}10^{-5}{}_{s}$
2	$1.06{\cdot}10^{-5}{}_{l}$	$4.22{\cdot}10^{-5}{}_{l}$
	Short-circuit $_{s}$	$5.65{\cdot}10^{-6}{}_{s}$
3	$5.10{\cdot}10^{-5}{}_{l}$	-
	$3.08{\cdot}10^{-3}{}_{s}$	-

These values are decreased by the contact resistance and would therefore be a minimum value for each pellet. As the calculated conductivity dropped consistently with about a factor of 10 from the long contacts to the short contacts, the contact resistance is presumed to be quite high since the dimensional factor A/l did not cause this difference as it was only 1-2 times higher for the short contacts.

9.5.1 The density of the pellets made for the conductivity measurements

The density of the two pellets made from the mixed powders calcined at 1150 ^{o}C which had the highest measured conductivity for batch 2 (more complexing agent) and 3 (more EG) was calculated to be 3.867 g/cm^3 and 3.296 g/cm^3, respectively. These values corresponds to 76 % and 65 % of the theoretical density of $CuAlO_2$ (5.097 g/cm^3) [37]. The color of the pressed and sintered pellets was grey for both batches, which can be seen in Figure 9.14. The same observation has been done by others [42].

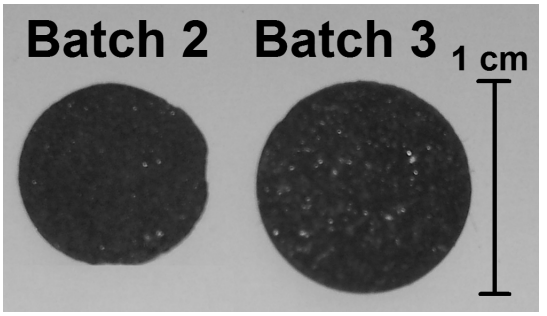

Figure 9.14: *The pressed and sintered pellet of batch 2 and 3.*

The microstructure in the cross-section of the pellets can be seen in the SEM images in Figure 9.15, showing that there are big pores in both pellets. The particles seems to be more sintered within the denser parts of batch 2 compared to batch 3 where smaller pores can be seen within the denser areas of the pellet. The element contrast (Z-contrast) in the BSE-signal shows that the pellets are not single-phase. The bright phase is probably $CuAlO_2$ while the darker phase is $CuAl_2O_4$ as heavier elements give a stronger signal than lighter elements [75]. Copper is heavier than aluminium giving $CuAlO_2$ a brighter appearance.

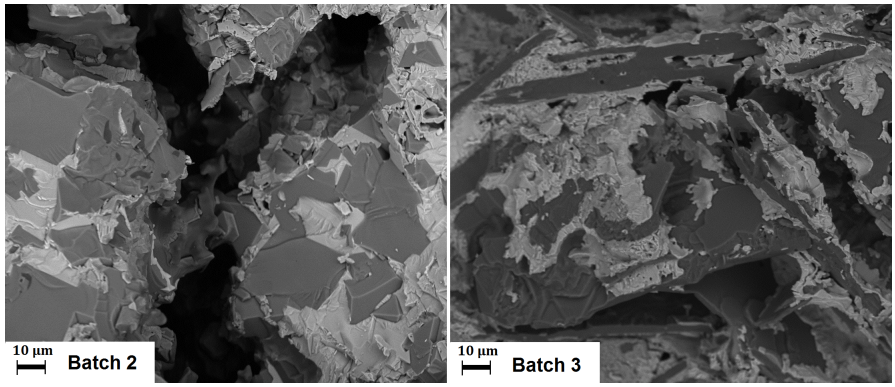

Figure 9.15: *The microstructure in the cross-section of the pellets from batch 2 and 3.*

10 The characterization of $NaLa(WO_4)(MoO_4)$:Eu

10.1 Observations during the syntheses

These observations were done by the author during the work for the preliminary master thesis [1]. The complexed Mo-precursor mixed well with the complexed W-precursor for both for malic acid and tartaric acid as complexing agents. The tartaric acid complexed solutions turned brown upon mixing of Mo- and W-precursors while the malic acid complexed solutions stayed clear. The addition of the complexed La-precursor had to be done very slowly for both malic acid and tartaric acid complexed solutions due to the formation of white lumps which needed some time to be dissolved again. This process was more challenging for the tartaric acid complexed solutions which turned brown/black upon this addition and more white lumps. The addition of EG did not affect the appearance of the solutions. The different solutions displayed many color changes during the evaporation and gelling process. The malic acid complexed solutions, denoted as syntheses NLMW-m and NLMW-mEG were yellow, but transparent. The solutions with tartaric acid were brown at first with white viscous substances swirling around in the bottom of the beakers. After some evaporation of water they became black, but partly transparent, and the white substances dissolved. The color difference at this stage is presented in Figure 10.1.

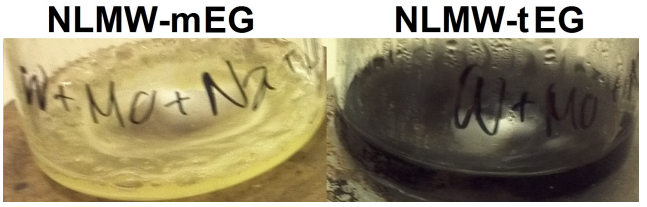

Figure 10.1: *The solutions of sample NLMW-m and NLMW-t just before gelling [1].*

As the water content became critically low during the last stages of the gelling, all the gels became yellow and opaque as seen in Figure 10.2.

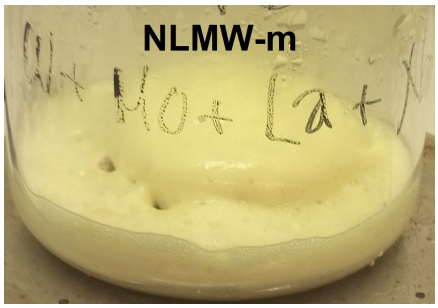

Figure 10.2: *The sample NLMW-m showing the general color of all the samples at the end of the gelling process just before self-ignition [1].*

As these viscous gels dried up, they self-ignited initiating smoldering reactions turning the gels into porous structures with a high volume increase, as seen in Figure 10.3.

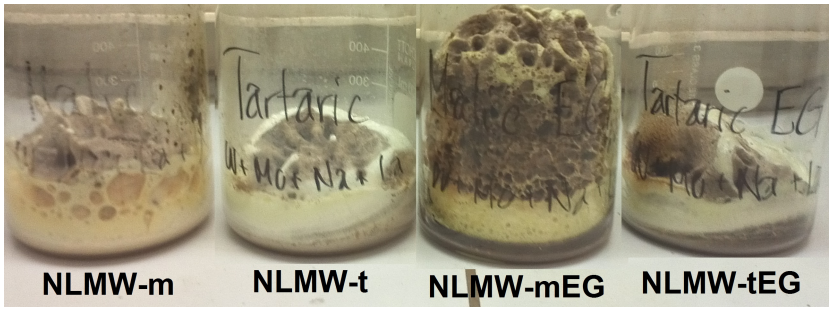

Figure 10.3: *Beakers with smoldered gels of Eu-doped $NaLa(WO_4)(MoO_4)$ [1].*

All these observations are summarized in Table 10.1.

Table 10.1: *Observations during the evaporation process of Eu-doped $NaLa(WO_4)(MoO_4)$ gels. The observations listed are the color of the initial stable solution, the color after gelling, the color after smoldering of the gel and the volume increase of the gels during smoldering.*

Gel	Color of sol.	Color of gel	Color of smold. gel	Volume increase
NLMW-m	Yellow	Yellow	Yellow/brown	Medium
NLMW-mEG	Yellow	Yellow	Yellow/brown	Large
NLMW-t	Brown/black	Yellow	White/brown	Medium
NLMW-tEG	Brown/black	Yellow	White/brown	Medium

The color of the calcined gels was black at 300 and 400 ºC, grey at 500 ºC and completely white at 600 and 1000 ºC. The tartaric acid complexed gels calcined at 500 ºC had a darker color compared to the malic acid complexed gels.

10.2 Phases present and crystallite size in the gels and calcined gels

The XRD spectra of the gels were obtained during a previous study [1], but have been analysed again during this work. Figure 10.4 is showing the analysed XRD spectra of these gels. The phases $WO_{2.95}$ and $La_{0.33}W_{0.67}O_7$ could be seen for NLMW-m, but many reflections could not be identified. Most of these unidentified reflections are most likely originating from an organic salt. The two strongest reflections for NLMW-m could also be seen in NLMW-t indicating traces of $La_{0.33}W_{0.67}O_7$ and the organic salt also for this sample. As the salt is present in both a malic acid and tartaric acid

complexed gel, this salt is probably not derived from the complexing agents. More reflections were present for the malic acid complexed gels compared to tartaric acid and the gels with no EG also had more reflections compared to the gels with EG, implying a higher crystallinity in the gels when fewer complexing and polymerizing groups are present in the gels.

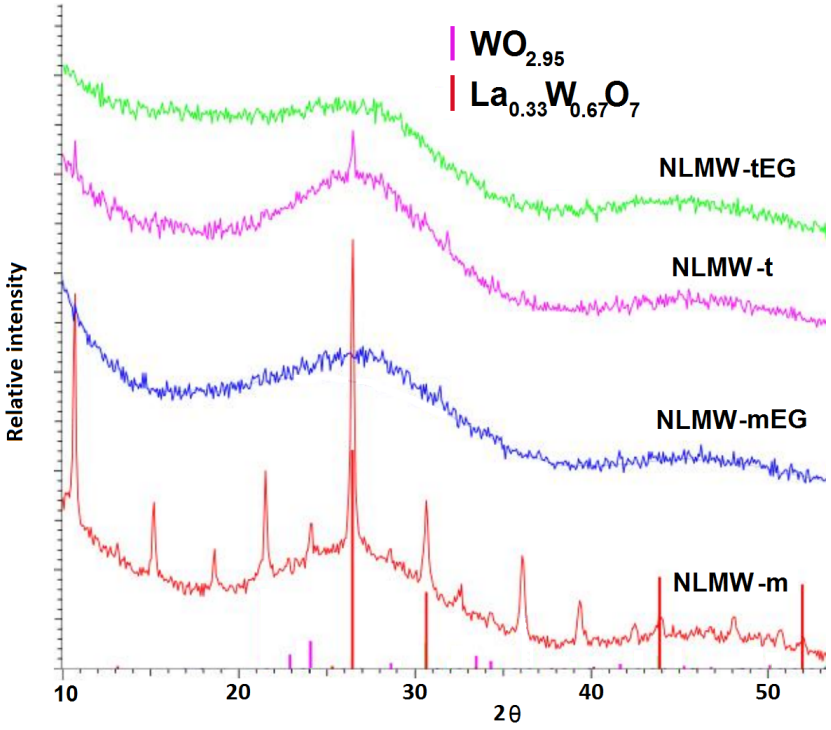

Figure 10.4: *XRD spectra of the uncalcined $NaLa(WO_4)(MoO_4)$ gels. Some reflections could not be identified.*

Figure 10.5 is showing the XRD spectra for the uncalcined NLMW-m gel and the powders calcined at 300, 400, 500, 600, 700 [1] and 1000 ºC and indicates the general trend of all the gels when calcined. The combination of

the phases $NaLa(WO_4)_2$ and $NaLa(MoO_4)_2$ gives the diffraction reflections for $NaLa(WO_4)(MoO)_4$ which is a solid solution of these two phases as described in Section 4.2.1. According to the XRD spectra, the samples calcined at 600, 700 and 1000 ºC contains pure $NaLa(WO_4)(MoO)_4$, while in the sample calcined at 500 ºC this is the dominating phase. Significant amounts of $NaLa(WO_4)(MoO)_4$ can also be seen for the samples calcined at 400 ºC. Some differences could be seen between the samples calcined at the same temperature. NLMW-m gave small reflections at 10.5, 21.2, 26.2 and 35.5 º in the XRD spectrum at 300 ºC indicating traces of some crystalline phases, while the other samples only had smooth diffractograms similar to the diffractogram for NLMW-m but without the reflections. At 400 ºC the differences in the diffractograms between the differently complexed samples had disappeared. At 500 ºC, traces of $WO_{2.95}$ could be seen for NLMW-m, which could not be observed for the other samples when calcined at this temperature. This was the only difference between the samples calcined at 500 ºC and no visible differences could be seen between the samples calcined 600, 700 and 1000 ºC.

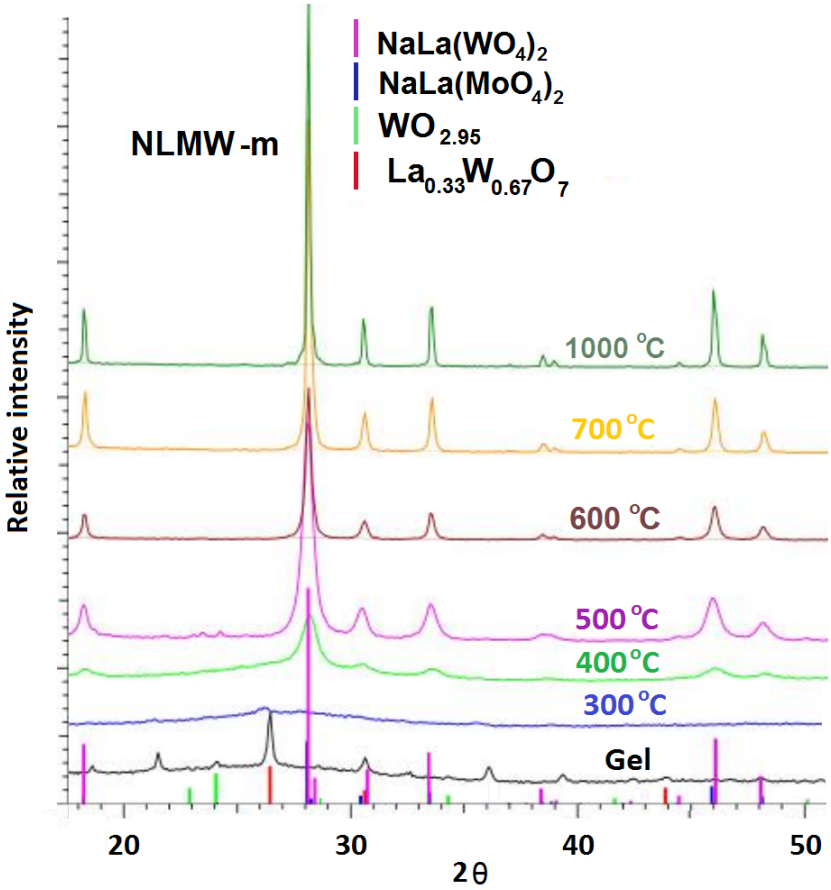

Figure 10.5: *XRD spectra of NLMW-m, uncalcined and calcined at 300, 400, 500, 600, 700 and 1000 ºC. The diffractograms for this sample are indicating the general trend for all the gels of $NaLa(WO_4)(MoO_4)$ when calcined.*

Table 10.2 is presenting the crystallite sizes of the calcined gels of $NaLa(WO_4)(MoO_4)$ at 500, 600, 700 and 1000 ºC. The values at 700 ºC

are taken from the preliminary master thesis work [1]. The crystallite sizes are increasing for increasing calcination temperatures.

Table 10.2: *Crystallite sizes of Eu-doped $NaLa(WO_4)(MoO_4)$ for the calcination temperatures 500, 600, 700 and 1000 ºC. The values at 700 ºC are taken from the preliminary master thesis [1]. All the values are given in nm.*

Gel	500 ºC	600 ºC	700 ºC [1]	1000 ºC
NLMW-m	12	22	30	43
NLMW-mEG	13	17	23	39
NLMW-t	13	20	29	46
NLMW-tEG	13	19	28	47

Figure 10.6 is showing the FT-IR spectra for of the uncalcined NLMW-m along with the calcined samples at 300, 400, 500, 600 and 700 ºC. The broad band between 3100-3600 cm^{-1} corresponds to the O-H stretching vibrations which can be seen in all the spectra [76]. The narrow peak at 1383 cm^{-1} is due to physically surface adsorbed NO_2 or CO_2 [77] which is present in all the spectra, but especially for the uncalcined gel. A band at 1636 cm^{-1} can be seen for the uncalcined gel and corresponds to the bending mode of lattice-coordinated H_2O [76]. This band is also present for the calcined samples but decreases in intensity with increasing temperature. The bands in the region 1250-1600 cm^{-1} originates from the degenerate ν_1 and υ_3 vibrational modes of NO_3^- [78]. The splitting may be caused by decrease in symmetry of the nitrate ion because of coordination with La. The band in the region 700-950 cm^{-1} may be due to MoO_4^{2-} [79, 80]. This band gets narrower and shows increasing intensity for increasing calcination temperature. The small band at 2850-3150 cm^{-1} visible for the uncalcined gel is due to C-H bonds and the small band at 2350 cm^{-1} comes from CO_2 and is visible for all the samples [79].

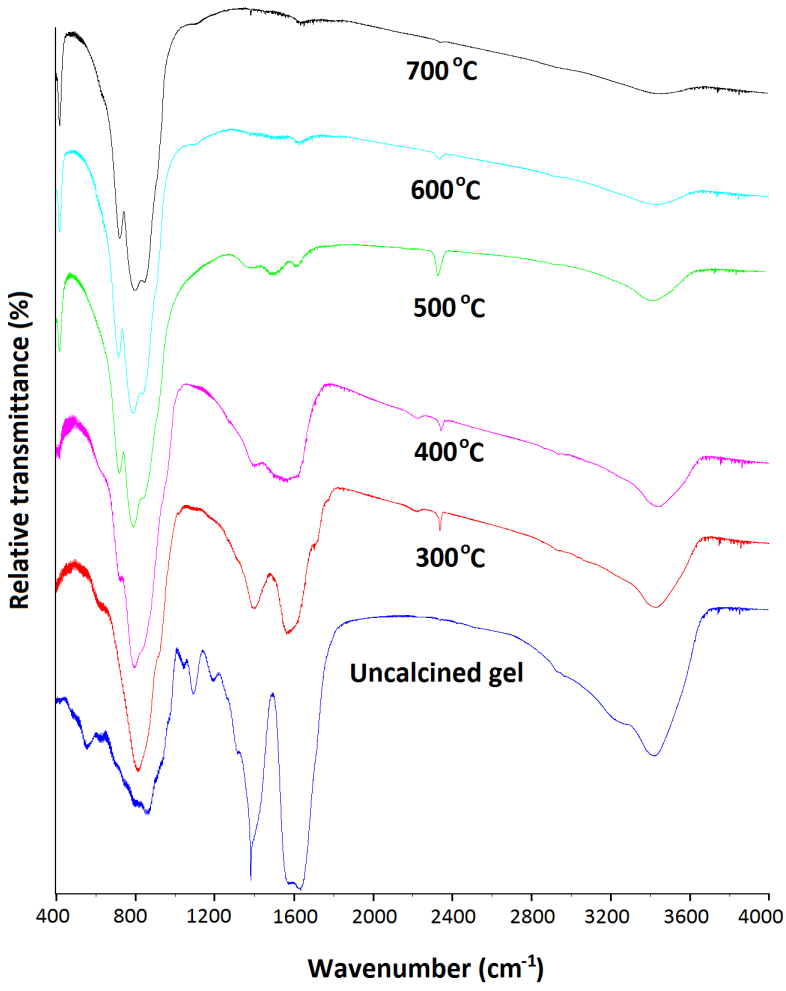

Figure 10.6: *FT-IR spectra of the NLMW-m uncalcined gel along with the calcined samples at 300, 400, 500, 600 and 700 ºC. The sample calcined at 700 ºC was produced as a part of a previous study [1].*

10.3 Loss of mass during calcination

Table 10.3 is presenting the remaining mass percentage after calcination at various temperatures for the $NaLa(WO_4)(MoO_4)$ gels. The mass is slowly reduced for increasing temperatures. At a calcination temperature of 500 ºC and above, the remaining mass percentage is quite stable, indicating that most of the impurities have burned off at 500 ºC.

Table 10.3: *The remaining mass in percentage after calcination in air at various temperatures for the $NaLa(WO_4)(MoO_4)$ gels. The values at 700 ºC is taken from at previous report by the author [1].*

Gel	300 ºC	400 ºC	500 ºC	600 ºC	700 ºC	1000 ºC
NLMW-m	69	66	59	59	59	58
NLMW-mEG	75	67	60	60	60	59
NLMW-t	72	68	62	62	62	59
NLMW-tEG	72	65	59	58	59	58

10.4 Particle size, surface area and morphology

The surface area of the 700 ºC calcined samples produced during a previous work [1], was measured by nitrogen adsorption and calculated by applying the BET-isotherm and these values are presented in Table 10.4. The surface area seems to be lower for the malic acid complexed calcined samples and the addition of EG seems to be lowering the surface area even more.

The NLMW-m and NLMW-t samples calcined at 700 ºC during the preliminary master thesis work [1] were imaged with SEM, and the images

obtained can be seen in Figure 10.7. The particle size, size distribution and particle shape appears to be similar for the two samples.

Table 10.4: *The surface area measured by nitrogen adsorption and calculated with the BET-isotherm for the 700 ºC calcined samples produced during a previous work [1].*

Calcined gel (700 ºC)	**Surface area (m^2/g)**
NLMW-m	6.6642 ± 0.0374
NLMW-mEG	5.3918 ± 0.0272
NLMW-t	7.6425 ± 0.0473
NLMW-tEG	5.7153 ± 0.0360

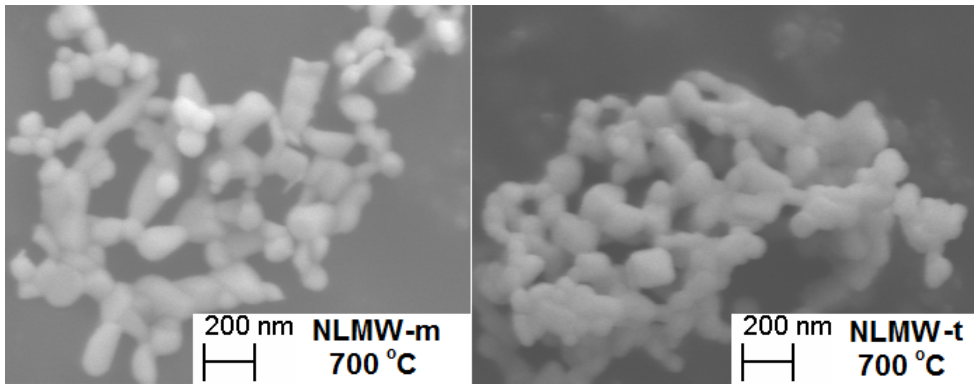

Figure 10.7: *SEM images obtained during a previous study [1] of the NLMW-m and NLMW-t calcined samples at 700 ºC.*

10.5 Photoluminescence

The photoluminescence emission spectra of the calcined NLMW-m sample calcined at various temperatures can be seen in Figure 10.8. The emission intensity at 615 nm is increasing with increasing temperature for the temperatures 400-600 ºC, while the 700 ºC calcined sample showed lower emission intensity compared to the 600 ºC calcined sample. All the samples were exposed to the same intensity of incoming light but the exposure times were 300, 25, 15 and 15 ms for the sample with calcination temperatures of 400, 500 600 and 700 ºC, respectively. The red and blue curves in Figure 10.8 are originating from different areas of different brightness in the samples, marked as red and blue squares in Figure 10.9 for each sample. These squares have been enlarged in the presented images due to visibility, being only about 5 μm in the original images. The position of the squares was selected to show the difference between the darker and brighter areas of each sample. Darker areas of poorer luminescent properties are dominating in the 400 ºC calcined sample, but the amount of bright luminescent phase is increasing with increasing calcination temperature up to 600 ºC. The lines in the spectra in Figure 10.8 are characteristic for Eu^{3+} and the transitions $^5D_0 \rightarrow {}^7F_1$, $^5D_0 \rightarrow {}^7F_2$, $^5D_0 \rightarrow {}^7F_3$ and $^5D_0 \rightarrow {}^7F_4$ are responsible for the lines at 590, 615, 652, 687-700 nm, respectively.

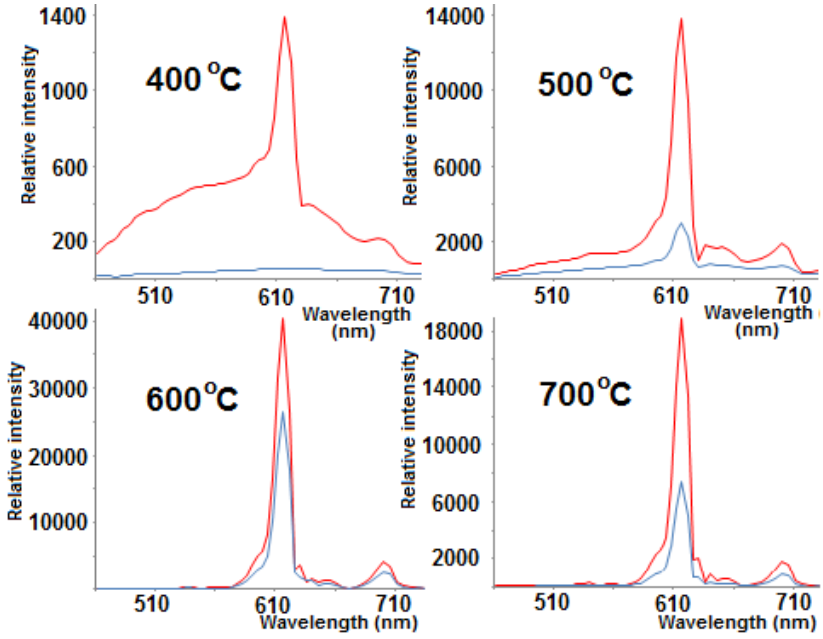

Figure 10.8: *Photoluminescence emission spectra of the NLMW-m sample calcined at various temperatures. The red and blue curves are giving the spectra measured within the red and blue squared in Figure 10.9. The exposure times were 300, 25, 15 and 15 ms for the samples calcined at 400, 500, 600 and 700 °C, respectively.*

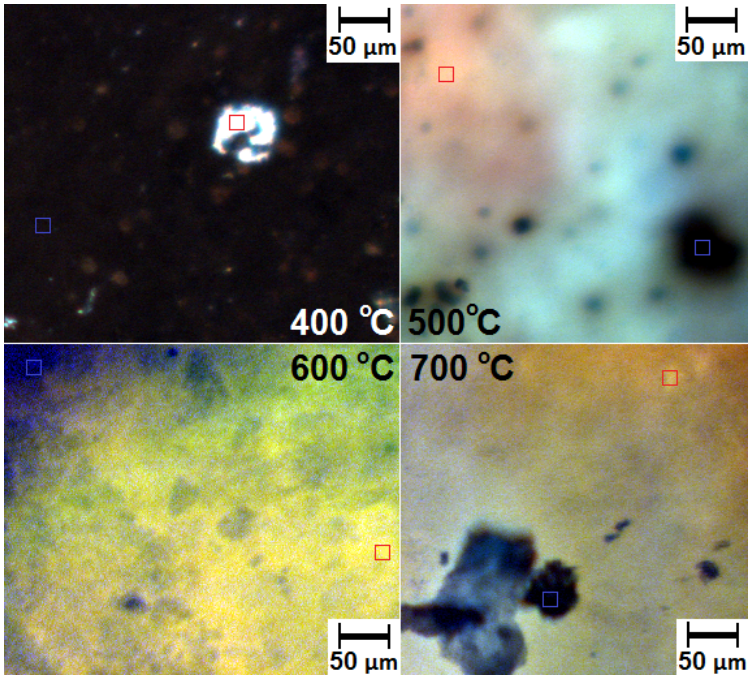

Figure 10.9: *Optical microscope images of the NLMW-m calcination series showing luminescent material and darker areas of poorer photoluminescent properties. The red and blue squares are giving the position from where the red and blue curves in Figure 10.8 are originating from. These squares have been enlarged in the figure for visibility reasons, being only 5 µm originally.*

Differences can be seen between the samples with different complexing agents and addition of EG when calcined at 500 ºC, as presented in Figure 10.10. The emitted light had a lower intensity for the tartaric acid complexed gels, which may be due to larger amounts of impurities. The color of the calcined powders may support this statement as described in Section 10.1.

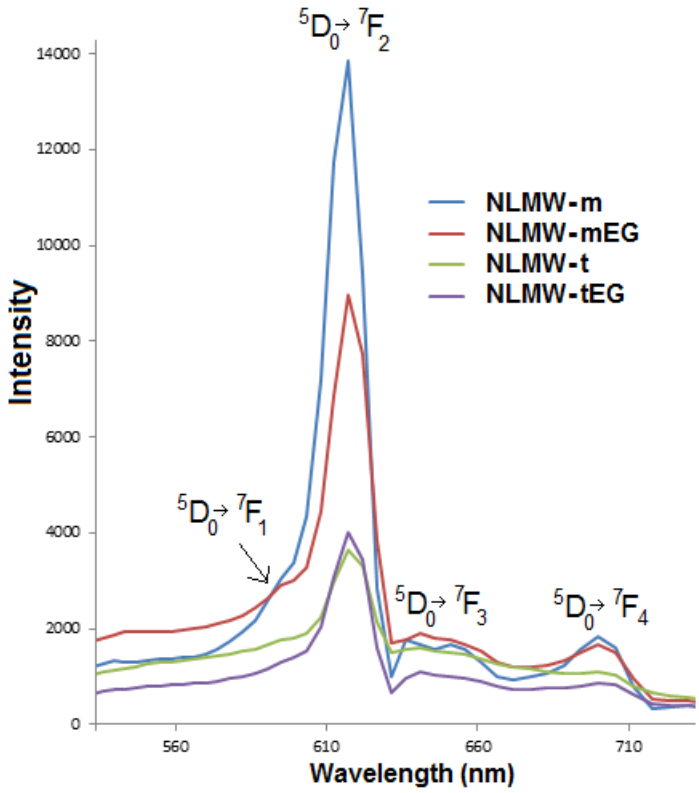

Figure 10.10: *Photoluminescence emission spectra of the 500 ºC calcined samples. The characteristic emission transitions of Eu^{3+} are given at each peak.*

The excitation spectra were measured for the sample NLMW-m calcined at 400, 500, 600 and 700 ºC [1] and are presented in Figure 10.11. The characteristic excitation transitions of Eu^{3+} are marked at each peak. The excitation intensity is increasing with calcination temperature, although a slightly lower intensity was measured for the 700 ºC calcined sample

compared to 600 ºC. The large excitation band at lower wavelengths in the spectrum is due to absorption in the host lattice.

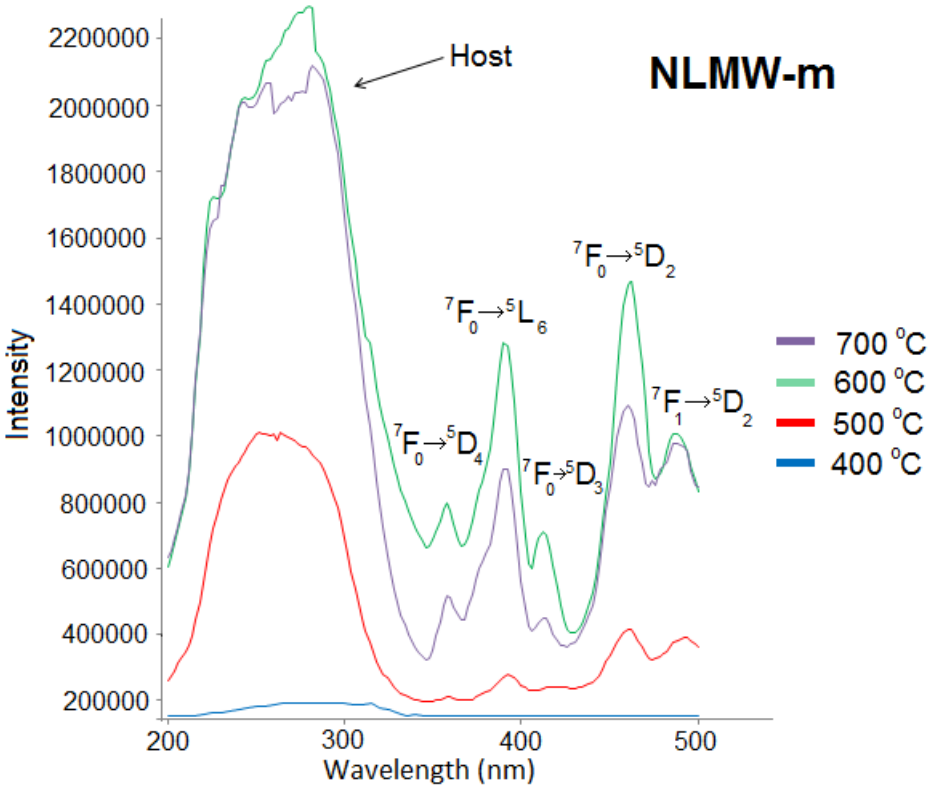

Figure 10.11: *Excitation spectrum of sample NLMW-m calcined at 600 ºC. The characteristic excitation transitions of Eu^{3+} are marked at each peak.*

Part V
Discussion

11 The synthesis of $CuAlO_2$

From the results in Section 9 it is obvious that the modified Pechini method is not yet ideal for the production of nanocrystalline $CuAlO_2$. Quite high temperatures are needed to create powders of $CuAlO_2$ and impurities of varying amounts are present in these powders. The challenge of the method lies in controlling the internal partial pressure of oxygen and temperature in the gels during self-ignition and calcination. The key may be related to the amount of complexing agent and polymerization agent added to the gels, correct gelling temperature and calcination atmosphere.

The wanted phase $CuAlO_2$ was obtained for batch 1-3 at a calcination temperature of 1150 ^{o}C in air. This is higher compared to calcination temperatures obtained by others, e.g Ghosh *et al.* who managed to produce nanocrystalline $CuAlO_2$ at 1000 ^{o}C [29] with the Pechini method. According to the XRD spectra of the calcined gels for batch 1-3 in Section 9.2, the phases $CuAl_2O_2$ and CuO were present as impurities in all the product powders along with some traces of a hexagonal form of $CuAlO_2$ with a P63/mmc space group. The microstructure of the pellets presented in Figure 9.15 supports these results for batch 2 (more complexing agent) and 3 (more EG) as at least two phases could be seen due to element contrast (Z-contrast) in the BSE signal. The brightest phase is probably $CuAlO_2$ and the darkest should therefore be $CuAl_2O_4$ as aluminium would give a weaker electron signal than copper.

All the batches calcined in air at 900 ^{o}C contained a mixture of $CuAl_2O_4$ and CuO which would suggest that the $CuAlO_2$ formed at 1150 ^{o}C is a product of the reaction in Equation 2 in Section 4.1 and that the CuO and $CuAl_2O_4$ impurities left in the $CuAlO_2$ powders are due to an incomplete reaction between these. From Table 9.2, 9.4 and 9.6, the CuO and $CuAl_2O_4$ impurities in the calcined gels at 1150 ^{o}C in air did not give equal molar fractions of copper and aluminium in the powders. These deviations are probably due to uncertainties in the calculations as the calculated phase ratios in the powders are highly approximate.

Longer calcination programs may not be the solution for removing these impurities as batch 1 (standard recipe) did not have fewer impurities compared to batch 2 (more complexing agent) and 3 (more EG) which were calcined for only 1 hour while batch 1 was calcined for 6 hours. As O_2 is on the right side in the reaction, a lower partial pressure of oxygen would drive the reaction to the right, but as seen in the XRD spectra for the calcination products of batch 4 (stoichiometric in nitrogen) in Figure 9.9, a too low partial pressure of oxygen may cause the samples to be reduced too much, not giving a straight-forward solution to this problem, either.

11.1 The effect of the complexing and polymerization agents

11.1.1 Effects seen when varying the hot-plate temperature

By varying the temperature of the hot-plates during the evaporation and gelling process one could see that a lower hot-plate temperature gave a lower probability of self-ignition and less apparent smoldering reactions in the gels which again would give smaller amounts of inorganic copper compounds. No precipitations could be seen in the solutions of batch 1 (standard recipe),

3 (more EG) and 4 (stoichiometric in nitrogen). The present phases in the gels of these batches were mostly inorganic according to the XRD spectra presented in Figure 9.2, 9.6 and 9.8. Batch 1 and 4 had the same hot-plate temperature during the evaporation process and the gels of these batches were quite similar, both with respect to appearance of the uncalcined gels, the width of the reflections in the XRD spectra and the phases present in the gels.

As precipitations were not seen for batch 1, 3 and 4, the phases in the XRD spectra of the gels probably formed during the smoldering reactions initiated during the gelling. This could be seen when comparing the XRD spectra for the gels of batch 1 and 2, which were synthesized at 100 and 80 ºC, respectively. Inorganic copper compounds with oxidation numbers of both +2, +1 and 0 were dominating in the gels of batch 1 (see Figure 9.2), and organic copper salts where copper had not been reduced were dominating in batch 2 (see Figure 9.4) along with precipitations of tartaric acid for the samples CA-3t and CA-4t. The larger amounts of complexing agents in batch 2 compared to batch 1 seemed to enhance the crystallinity and the same effect was also seen when comparing the gels within this batch, especially for the gels without EG, see Figure 9.4. This increase in crystallinity was mainly due to precipitation of tartaric acid during the evaporation of the solutions, and the amount of precipitates increased with increasing amounts of tartaric acid added to the sols. This statement is supported by the observations done during the synthesis of this batch as white precipitations could be seen in these gels, see Section 9.1.

The gels of batch 3 were synthesized with a hot-plate temperature of 80 ºC. The gels contained quite large amounts of metallic copper in addition to the copper oxalate hydrate, except for the sample CA-2m-15EG which self-ignited resulting in a gel which resembled the gels of batch 1 containing

mostly CuO and Cu_2O. As this batch was synthesized with the same hot-plate temperature as batch 2, the enhanced formation of metallic copper compared to batch 2 was probably due to the large amounts of EG in this batch. The hot-plate temperature is thus not the only parameter affecting the probability of smoldering reactions in the gels. As more material can be burned off in the gel, more reducing conditions can be obtained, as in accordance with the phase diagram in Figure 4.1 and this may be the cause of the formation of metallic copper in these gels. The amount of material burned off during the smoldering reactions could easily be associated with the percentage of remaining mass after the calcinations, as a smaller amount of material would burn off during calcination if most of it had already been removed during the smoldering during the gelling. According to Table 9.10, this relationship is clearly stated as sample CA-2m-15EG, which was the only sample that self-ignited during gelling for this batch, had the highest remaining mass percentage after calcination at various temperatures.

As the XRD spectra of the gels in batch 3 in Figure 9.6 showed a mixture of copper oxalate hydrate and metallic copper for three of the gels. The reduction reaction happening during the smoldering must have been very local as the formation of metallic copper needs very high temperatures according to the phase diagram in Figure 4.1, while copper oxalate hydrate dehydrates around 180 ºC and decomposes at a temperature of 260 ºC [81] stating that the gels did not reach equilibrium during the reduction reactions. These very different conditions inside the gels could possibly be explained by the high amounts of EG, making the gels more viscous and less thermally conducting as EG has a higher viscosity than water and about 1/3 of the thermal conductivity compared to water [82, 83], confining the reducing conditions to local areas of the gel. The fact that EG did not burn off completely in this batch as the gels needed to be dried in a drying

cabinet after gelling, as described in Section 9.1, supports the proposed explanation as it must have been present in quite large amounts during the gelling.

The hot-plate temperature is very important for the final composition of the uncalcined gels and the phases present in them will affect the reactions occurring at different calcination temperatures. By comparing the content of metallic copper in the gels in Tables 9.1, 9.3 and 9.5 with the amount of produced $CuAlO_2$ for a calcination temperature of 1150 ^{o}C presented in the Tables 9.2, 9.4 and 9.6, one may draw the conclusion that less metallic copper in the gels will result in more $CuAlO_2$ for this calcination temperature. The effect of CuO and Cu_2O in the gels is not very clear, but it might seem that the presence of these phases in the gels would enhance the production of $CuAlO_2$ during calcination at 1150 ^{o}C. This statement is supported by Equations 1, 2 and 4 in Section 4.1.1 where CuO and Cu_2O acts as reactants for making $CuAlO_2$. By looking at the gel compositions in batch 3 in Figure 9.6, this assumption could be supported as the sample having the highest amounts of CuO and Cu_2O, CA-2m-15EG, gave the highest percentage of $CuAlO_2$ for a calcination temperature of 1150 ^{o}C in air. This high amount of $CuAlO_2$ could also be explained with the low amount of metallic copper in this gel compared to the other gels in this batch but lower amounts of metallic copper would also make it possible to have more CuO and Cu_2O.

During the evaporation of the solutions of batch 2 (more complexing agent), white precipitations could be observed in the solutions complexed with tartaric acid. This is not strange as tartaric acid has a solubility of 20.6 g/100 ml of water at 25 ^{o}C [84] and both gels with tartaric acid exceeded this solubility limit. These precipitations were visible in the XRD spectra for these gels as seen in Figure 9.4. According to these spectra more tartaric

acid would precipitate when more of this complexing agent was added to the solutions. Malic acid did not precipitate in the gels complexed with this complexing agent as it has a solubility of 55.8 g/100 ml of water at 25 ºC [85] and this solubility limit was not exceeded.

11.1.2 Effects seen when varying the calcination temperature

During calcination of the gels the crystallinity increased with increasing temperature for all the samples. This is clearly seen from the crystallite sizes in the powders, as described in Section 9.2 which increased with increasing temperature. To maintain as small crystallites a possible, the temperature should therefore be as low as possible when making the material. This could increase the challenge of making nanocrystalline $CuAlO_2$ as the method only has been successful for calcination in air at the highest calcination temperature, 1150 ºC, during this study. For batch 4 which was calcined in nitrogen, the calcination temperature was too high giving metallic copper in dominating amounts already at 600 ºC.

For batch 1-3, the calcination temperatures 500-1000 ºC would first give CuO at the lowest temperature and then increasing amounts of $CuAl_2O_4$ with increasing temperature. Batch 1 (standard recipe) was calcined at 500 ºC for 1 hour which gave only CuO, but according to the XRD spectra of the gels of batch 1 in Figure 9.2, differences were seen between the samples with different complexing agents when they were calcined at 600 ºC. The use of malic and tartaric acid resulted in less metallic copper in the uncalcined gels compared to malonic acid as complexing agent and the sample CA-2t-2EG was the only sample giving traces of $CuAl_2O_4$ at a calcination temperature of 600 ºC in air when the other samples gave only

CuO. This is indicating that this sample was more homogeneous compared to the other samples in this batch making a reaction between copper and aluminium more probable. This sample also gave the highest amount of $CuAlO_2$ when calcined in air at 1150 ºC. These observations are indicating a similar trend as found by Selbach *et al.* [3] and Liu *et al.* [32], as described in Section 3.1. They found that an increasing amount of hydroxyl groups on the complexing agent would complex the softer cations better, reducing the probability of the cations to go into crystalline phases. As Cu^{2+} cations are on the borderline to being soft, while Al^{3+} cations are hard, the hydroxyl groups are critical for a successful complexation of copper in the gels.

In batch 2 (more complexing agent), none of the uncalcined gels had metallic copper in them and after the calcination at 600 ºC all the gels contained some $CuAl_2O_4$. This confirmes the trend seen for batch 1 where a lower amount of metallic copper in the gels gave higher amounts of $CuAl_2O_4$ at lower calcination temperatures. The two gels in batch 2 which had a small addition of EG (CA-3m-1EG and CA-4m-1EG) had the highest percentage of $CuAl_2O_4$ compared to the gels without EG which only had traces of this phase. This addition of EG gave less copper-containing crystalline phases and thus seems to be important for the homogeneity of the gels. The gels in batch 3 (more EG) had, on the contrary, much larger amounts of metallic copper compared to batch 1 and 2 according to Figure 9.6, giving them a much lower homogeneity, which would explain why no $CuAl_2O_4$ was formed before 900 ºC in this batch.

The observations of the relationship between metallic copper in the uncalcined gels and the production of $CuAl_2O_4$ and $CuAlO_2$ during calcination at different temperatures can be explained by the homogeneity of the gels. As described in Section 3.1, the different ions have different chemical properties, affecting the complexing agent's ability to complex them. From

the XRD spectra of the uncalcined gels of the batches of $CuAlO_2$ in Section 9.2, one could see that the crystalline phases present in the gels were generally copper compounds which could be explained by the fact that Cu^{2+} cations are softer than Al^{3+} giving the hard hydroxyl and carboxyl groups a better opportunity to complex the aluminium cations. The presence of crystalline copper compounds in the gels would give a lower homogeneity since copper and aluminium would be present in separate phases, reducing the possibility of having reactions between these two elements.

For batch 1 (standard recipe) and 2 (more complexing agent), the addition of EG varied from gel to gel and the addition of EG seemed to have a positive effect on the homogeneity in the gels as the crystallinity and the amount of metallic copper compared to the other phases decreased in these gels. This could be explained by an enhanced gel formation when EG was added. But a too large addition of EG would cause other effects to occur as in batch 3 (more EG), where large amounts of metallic copper could be seen in the uncalcined gels (except for in CA-2m-15EG) giving a low homogeneity. The $CuAl_2O_4$ phase was therefore not formed before 900 ^{o}C in this batch. In the gels of batch 3, the EG possibly acted more as a reduction agent than a polymerization agent, due to the large amounts of it, making the gels more inhomogeneous. This is supported by the traces of Cu_2O in sample CA-2t-30EG when calcined at 600 ^{o}C showing that more reducing conditions could be seen for this batch as copper was not reduced for any of the other batches at this calcination temperature.

According to the SEM images obtained for the 1150 ^{o}C calcined gels of batch 1 (standard recipe) and 3 (more EG) in Section 9.4, the smallest particles found in batch 1 were in the range of 15-20 nm, as seen in Figure 9.10 while the smallest particles found in batch 3 were at least 10 times this size as seen in Figure 9.13. As the crystallite sizes of the calcined

powders in these batches were quite similar, as described in Section 9.2 a more extensive agglomeration must have taken place in batch 3, possibly being enhanced by the large amounts of EG present. The SEM images in Figure 9.13 also presents a difference in the particle size when using different complexing agents in batch 3. Larger particles can be seen for the sample complexed with tartaric acid, indicating that a larger complexing agent will give larger particles.

11.1.3 Effects seen when varying the calcination atmosphere

The use of reduced partial pressure of oxygen in the furnace during calcination caused the gels to be reduced too much, giving mostly metallic copper as seen in Figure 9.9 for a calcined sample of batch 4. Metallic copper was formed in the gels already at 600 ºC due to the nitrogen atmosphere. The gel with the lowest amount of added material to be burned off, according to molar mass, was sample CA-0.5mn-1EG and this was the only gel that showed traces of $CuAlO_2$. These traces could be seen for a calcination temperature of 800 ºC and was probably formed through the reaction in Equation 4 in Section 4.1.1 as Cu_2O was found in the uncalcined gel and also after calcination at 600 ºC. No signs of $CuAlO_2$ could be found for a calcination temperature of 600 ºC. This can be explained by the increased mobility of the cations at 800 ºC compared to 600 ºC increasing the possibility of a reaction between copper and aluminium. Also the increased total time of the calcination program for a calcination temperature of 800 ºC gives the reaction more time to occur. For samples CA-0.75mn-1EG and CA-1mn-1EG, too reducing conditions would appear in the gels during calcination due to the larger amounts of additives compared to CA-0.5mn-

1EG, as more material would have to be burned off producing more carbon to reduce the copper. This was also the case for the samples complexed with malic and tartaric acid in this batch. The ideal reaction described by Equation 5 in Section 5.2.1 is thus not giving the actual reaction in the gels during calcination as a lower α-value than predicted is needed. As parts of the reaction are occurring during the smoldering reaction in air, such an ideal reaction is hard to estimate.

11.2 The effect of density and impurities on the electrical conductivity

The data from the electrical conductivity measurements in Section 9.5 reveiled a conductivity of of $3.1 \cdot 10^{-3}$ S/cm for one of the sintered pellets from batch 2. The electrical conductivity obtained by Thu *et al.* for sintered undoped pellets [42], was only 2.5 times this value and was obtained for a pellet with 87 % density compared to a density of only 76 % for the pellet from batch 2. The pellet from batch 3 had an even lower conductivity of only $1.0 \cdot 10^{-4}$ S/cm and the density of this pellet was only 65 %. Also, these conductivities include a contact resistance, which was assumed to be quite high.

The obtained densities for the sintered pellets of $CuAlO_2$ were quite low as described in Section 9.5.1 with a lower density for batch 3 compared to batch 2. The microstructure of the pellets presented in Figure 9.15 showed that large pores were present in both pellets. The pellets seemed to have sintered well within the agglomerates, especially for batch 2, leaving large pores to be formed between these agglomerates. Ball milling before pressing of the pellets should be employed to reduce this effect. The lower calcu-

lated density for the pellet from batch 3 might explain why the measured conductivity was lower for batch 3, as seen in Section 9.5, although the calculated amount of $CuAlO_2$ in the batches was slightly higher in batch 3. As described in Section 4.1.2, elevated amounts of $CuAl_2O_4$ impurities will degrade the electrical properties of $CuAlO_2$.

The highest measured electrical conductivity was only 1/2.5 of the reported value for undoped pellets [42]. Both impurities, low densities and high contact resistances were degrading the measured electrical conductivity of the pellets, and if these factors were to be improved, the modified Pechini method could possibly give pellets of higher measured electrical conductivity and thus be a promising way of producing $CuAlO_2$.

11.3 Outlook

Many parameters in the modified Pechini method were studied in this work and some alterations to the synthesis route can be suggested based on the results of using these. For the synthesis of $CuAlO_2$, the employment of a pure nitrogen atmosphere during calcination, gave too reducing conditions for quite a large range of temperatures for the set of precursors used and the type of complexing agent and polymerization agent chosen in this work. A very low calcination temperature should therefore be used (possibly below 600 ^{o}C) along with very small additions of complexing and polymerization agents. Such a low calcination temperature might give problems with getting rid of all the organic additions in the gels, resulting in impurities such as carbon residues in the gels. Employing a mixed external atmosphere with for instance a mixture of oxygen and argon could in theory give a solution to the problem of a too reducing atmosphere, but as the partial

pressure of oxygen in this range is very hard to control, this could give a synthesis method with highly uncontrollable results.

For calcination in air, one would have to go higher in calcination temperature to be able to remove $CuAl_2O_4$ and CuO impurities. Milling of the powders could also help with reducing these impurities as found by Deng *et al.* [36]. The use of other types of precursors has also shown to be helpful in obtaining $CuAlO_2$ as Ghosh *et al.* showed that a calcination temperature of 1000 ºC in air was high enough to give pure $CuAlO_2$ when using nitrate precursors for both copper and aluminium in the Pechini method [29] and the same trend was also seen in the work of Li *et al.* [4].

Ren *et al.* had success for a calcination temperature of 900 °C in nitrogen for $CuAlO_2$ films made with the same cation precursors as in this work, acrylic acid (AA) as complexing agent and isopropyl alcohol (IPA) as polymerizing agent [28]. This shows that they were able to obtain less reducing conditions in the gels during calcination in nitrogen compared to the gels in this work (batch 4). Ren *et al.* added 100 times more of the polymerization agent compared to the samples calcined in nitrogen in this work and such an addition would, according to Section 5.2.1, cause the conditions in the gels to be more reducing compared to lower amounts of polymerization agent. This was seen for the gels in batch 3, where the larger amounts of EG in one of the gels gave more reducing conditions during calcination at 600 ºC in air. This example is not completely comparable to calcination in nitrogen, but the trend is still clear. For a better understanding of this apparent inconsistency, the type of polymerization agent should be investigated according to its ability to reduce the gels. The less reducing conditions in the work of Ren *et al.* could also be due to an easier escape of the nitrous and carbonaceous gases evolving in the gels, thus letting more oxygen be present in the gels as they dip-coated the gels onto

substrates before calcination making the samples thinner than in this work. This effect should also be investigated.

12 The synthesis of $NaLa(WO_4)(MoO_4)$:Eu

The modified Pechini method using malic acid and tartaric acid as complexing agent has proven to be an excellent method for producing Eu-doped $NaLa(WO_4)(MoO_4)$ at very low temperatures. Already at 400 °C, traces of the wanted phase was identified and at 500 °C only traces of impurties were present in the diffractograms. At 600 °C a single-phase nanocrystalline oxide was obtained and the same pure phase was obtained for calcination temperatures of 700 and 1000 °C, although the crystallite size increased.

During the evaporation process, no precipitations were observed in the gels after the gelling had occurred. Tartaric acid gave the lowest degree of crystalline phases in the gels, by comparing the XRD spectra of the gels in Figure 10.4, and the addition of EG reduced the crystallinity even more for both complexing agents. The most critical part during the synthesis was the complexation of each cation and the mixing of these to make a stable solution. The gelling occurred at different stages in the evaporation process, but all the solutions had polymerized making a homogeneous gel before the smoldering reaction started.

12.1 The effect of the complexing and polymerization agents

The XRD spectra presented in Figure 10.4 showed that tartaric acid gave a lower degree of crystallinity in the gels making the gels more homogeneous

when using this complexing agent. Tartaric acid may therefore be a better complexing agent than malic acid for this system. But the color differences between the calcined samples at 500 ^{o}C indicated that tartaric acid needed a higher calcination temperature compared to malic acid to be burned off completely. The photoluminescence emission intensity also was lower in the gels complexed with tartaric acid compared to malic acid for a calcination temperature of 500 ^{o}C, supporting that more impurities were present in the tartaric acid complexed gels. This may, for instance, be due to smaller pores in the gel, trapping the tartaric acid more strongly. Such impurities are hard to detect with XRD, and therefore the XRD results can not rule out this possibility.

The color changes in the mixed solutions during the evaporation process as described in Table 10.1, showed a tendency for malic acid to enhance gelling at an earlier stage in the evaporation process compared to tartaric acid, as the yellow color of the gel appeared earlier. According to the XRD spectra in Figure 10.4, all the gels were mostly amorphous, but a lower degree of crystallinity was observed in the two gels complexed with tartaric acid compared to malic acid. The cations in $NaLa(WO_4)(MoO_4)$ are classified as hard according to Table 3.2. The hardness of the cations may have enhanced the complexing as both the hydroxyl and carboxyl groups are hard. As tartaric acid has more complexing groups, this may be the reason for the lower crystallinity in the gels complexed with tartaric acid. The addition of EG also resulted in a lower degree of crystallinity in the gels for both complexing agents which was probably due to the formation of a more rigid gel network.

Two of the crystalline phases seen in the uncalcined gels could be identified as $La_{0.33}W_{0.67}O_7$ and $WO_{2.95}$. The most intense reflection in the NLMW-m sample was due to to the $La_{0.33}W_{0.67}O_7$ phase and this reflec-

tion could also be seen for the NLMW-t sample. Both of these samples also had a reflection at 11 º, being most apparent in the NLMW-m sample. This reflection was the strongest reflection of a crystalline phase which could not be identified, but probably was originating from an organic salt. The IR spectrum for the uncalcined NLMW-m gel seen in Figure 10.6 is not ruling out this possibility, as the signal from both O-H and C-H bonds is present in this spectrum. This salt is probably not derived from the complexing agents, as it is appearing in both the malic acid and tartaric acid complexed gels.

Although the degree of homogeneity was quite different for the uncalcined gels, these differences started to dissapear already at quite low calcination temperatures. At 300 ºC, the XRD spectra of the samples appeared very similar, except for a few reflections of an unidentified crystalline phase in the NLMW-m sample which did not appear for the other three samples. As seen in Figure 10.5, these reflections dissapeared at 400 ºC, and for 500 the samples seemed identical except for traces of $WO_{2.95}$ for NLMW-m calcined at 500 ºC. At 600, 700 [1] and 1000 ºC the samples were similar with only $NaLa(WO_4)(MoO_4)$ as the present phase. This is supported by the percentage of remaining mass of the samples at various calcination temperatures in Table 10.3. Above a calcination temperature of 500 ºC, the remaining mass was relatively stable with increasing temperature. These observations are supported by the IR spectra in Figure 10.6, showing decreasing intensities for the bands representing O-H bonds, physically adsorbed CO_2/NO_2, lattice-coordinated H_2O, NO_3^- and C-H bonds when the temperature is increasing, while the band representing vibrations in MoO_4^{2-} is getting narrower and more intense when the temperature increases. For the samples calcined at 600 and 700 ºC, only small bands indicating traces of H_2O, CO_2 and O-H bonds were seen which probably were originating

from the adsorption of water and CO_2 after calcination, indicating that the purity of the $NaLa(WO_4)(MoO_4)$ in these samples is close to 100 %.

12.2 The effect of temperature and volume increase during gelling

After the polymerization had occurred and the water content became critically low, the gels self-ignited and Table 10.1 states that the sample NLMW-mEG had the largest volume increase during the smoldering of the gel. This may have resulted in a less dense gel compared to the others, which again would inhibit the growth of crystallites during calcination. This is supported by the crystallite sizes given in Table 10.2 which gave the smallest crystallite size for this gel at calcination temperatures of 500, 600 and 700 ºC. On the contrary, the surface area of the samples calcined at 700 ºC given in Table 10.4 gave the smallest surface area for NLMW-mEG, stating that the particles were larger in this sample. This is probably due to more extensive agglomeration in this sample during calcination.

According to the theory in Section 5.2.1, grain growth is enhanced when the temperature in the smoldering reaction increases, which would indicate that the temperature in the synthesis of NLMW-mEG was higher compared to the other gels. This statement could be supported by the percentage of mass loss during the calcinations seen in Table 10.3. For the tartaric acid complexed gels the remaining mass percentage was lower for NLMW-tEG which would be reasonable as EG is burned off in addition to the tartaric acid in this sample. This trend was opposite for malic acid complexed gels, suggesting that more material had been burned off, i.e. a higher

temperature hed been reached, during the synthesis of the NLMW-mEG sample.

12.3 The photoluminescence characteristics

All the calcination temperatures gave samples with a strong emission line at 615 nm, but especially at 600 and 700 ºC as seen in Figure 10.8. All these spectra were measured with an excitation wavelenth of 405 nm, but according to the excitation spectra for NLMW-m calcined at 400, 500, 600 and 700 ºC as seen in Figure 10.11, a stronger excitation line was measured for the samples at 465 nm. The intensity of the measured emission could thus have been higher if measured using an excitation wavelength of 465 nm. The excitation spectra for the calcined NLMW-m sample also showed high absorption in the host material which is not ideal for making a good red phosphor.

The emission intensity of the 600 ºC calcined sample was about twice as high compared to the 700 ºC sample. If this effect was due to small amounts of secondary phases obtained at 700 ºC, such phases would be more apparent for the samples calcined at 1000 ºC. But no such phases could be seen in any of the XRD spectra for the gels calcined at 700 or 1000 ºC and thus the lower intensity of the photoluminescence for the sample calcined at 700 ºC is probably due to inhomogeneities in the pellets made for these measurements. Such inhomogeneities could, for instance, be caused by slight differences pressure and holding time used for the pressing of the pellets. As the size of the area giving the emission spectra for the photoluminescence was only 5 μm, as described in Section 10.5, such inhomogeneities

could easily affect the measured intensities as they only represent one small point in the sample.

12.4 Outlook

The modified Pechini method worked quite well for the production of $NaLa(WO_4)(MoO_4)$ and two complexing agents have shown to be successful in the complexing of the cations. As the scheelite structure for this material was so easily obtained and the doping of Eu^{3+} was well integrated in this structure, higher percentages of doping should be investigated, possibly giving a stronger emission of red light for the material.

Part VI
Conclusions

The $CuAlO_2$ phase with the delafossite structure was obtained for the modified Pechini method using the complexing agents malonic, malic and tartaric acid for a calcination temperature of 1150 ºC in air for three different gel recipes. This has expanded the options for suitable complexing agents for the modified Pechini method. The highest measured electrical conductivity for $CuAlO_2$ in this work was 3.1 $\cdot 10^{-3}$ S/cm for a pellet pressed on powders made with elevated amounts of complexing agent.

Tartaric acid as complexing agent seemed to enhance formation of mixed metal oxides at lower temperatures. Larger amounts of complexing agents did not give clear advantages for the complexation of the cations but a small amount of polymerization agent gave enhanced gel formation with less precipitation of excess amounts of complexing agent and more amorphous gels with lower amounts of metallic copper. Less metallic copper could also be seen for a lower hot-plate temperature during gelling for moderate additions of EG, which also resulted in enhanced formation of mixed metal oxides at lower temperatures. A large addition of EG to the gels gave large amounts of metallic copper as more organic material could be burned off during the heat treatments causing oxygen to be expelled from the gels.

All the $CuAlO_2$ powders from calcination at 1150 ºC in air had impurities of $CuAl_2O_4$ and CuO and small traces of a hexagonal variant of $CuAlO_2$ with a P63/mmc space group. The highest purity of $CuAlO_2$ was achieved for a sample in batch 3 of 91 mass%. The $CuAlO_2$ formed in these samples was probably the result of a reaction between $CuAl_2O_4$ and CuO

as these phases were present in all the samples calcined at temperatures of 900 and 1000 ºC.

Small amounts of delafossite $CuAlO_2$ could also be found in addition to metallic copper and γ-Al_2O_3 in one of the samples calcined in nitrogen atmosphere at 800 ºC. This sample had the lowest amount of organic material to be burned off as the complexing agent with the smallest molar mass, malonic acid, was used in this gel and the concentration of malonic acid was the smallest of the samples in this batch. As the rest of the samples calcined in nitrogen at this temperature contained only metallic copper and γ-Al_2O_3, the general conditions were too reducing.

Single-phase nanocrystalline $NaLa(WO_4)(MoO_4)$ with Eu^{3+}-doping and with the scheelite structure was successfully synthesized with the modified Pechini method using malic and tartaric acid as complexing agents. The pure oxide was obtained for calcination in air at 600 and 1000 ºC but the wanted phase could also be seen for a calcination temperature of 400 and 500 ºC, although with higher amounts of impurities. The addition of EG decreased the degree of crystallinity in the uncalcined gels and tartaric acid as a complexing agent also had the same effect compared to malic acid. A strong photoluminescence emission line at 615 nm was seen for the Eu-doped $NaLa(WO_4)(MoO_4)$ phase and the intensity increased with increasing calcination temperature. Smaller crystallites after calcination could be observed for a sample containing EG and complexed with malic acid, which had the largest volume increase during gelling.

References

[1] S. L. Skjærvø, M.-A. Einarsrud, and T. Grande. Complex formers in wet chemical synthesis of oxides. Technical report, Norwegian university of science and technology, 2012.

[2] V. Gil, R. A. Strøm, L. J. Groven, and M.-A. Einarsrud. $La_{28\text{-}x}W_{4+x}O_{54+3/2x}$ powders prepared by spray pyrolysis. *Journal of American Ceramic Society*, 95(11):3404–3407, 2012.

[3] S. M. Selbach, M.-A. Einarsrud, T. Tybell, and T. Grande. Synthesis of $BiFeO_3$ by wet chemical methods. *Journal of the American Ceramic Society*, 90(11):3430–3434, 2007.

[4] K. Li, J. F. Huang, L. Y. Cao, B. Wang, and Z. Y. Shi. Preparation and optical properties of $CuAlO_2$ microcrystallites by complexing sol-gel. *Journal of Inorganic Materials*, 26(3):275–280, 2011.

[5] M. Nazarov and D. Y. Noh. *New Generation of Europium and Terbium Activated Phosphors: from syntheses to applications.* Pan Stanford Publishing Pte. Ltd., 2011.

[6] B. L. Cushing, V. L. Kolesnichenko, and C. J. O'Connor. Recent advances in the liquid-phase syntheses of inorganic nanoparticles. *Chemical Reviews*, 104(9):3893–3946, 2003.

[7] D. W. Richerson. *Modern Ceramic Engineering - Properties, processing and use in design.* Taylor and Francis, Boka Raton, USA, 3 edition, 2005.

[8] C. Brechignac, P. Houdy, and M. Lahmani. *Nanomaterials and Nanochemistry.* Springer, Berlin, Germany, 1 edition, 2006.

[9] N. Chandra. Constitutive behavior of superplastic materials. *International Journal of Non-Linear Mechanics*, 37:461–484, 2002.

[10] G. Thomas. Invisible circuits. *Nature*, 389:907–908, 1997.

[11] H. Kawazoe, M. Yasukawa, H. Hyodo, M. Kurita, H. Yanagi, and H. Hosono. P-type electrical conduction in transparent thin films of $CuAlO_2$. *Nature*, 389:939–942, 1997.

[12] A. Kudo, H. Yanagi, K. Ueda, H. Hosono, H. Kawazoe, and Y. Yano. Fabrication of transparent p-n heterojunction thin film diodes based entirely on oxide semiconductors. *Applied Physics Letters*, 75:2851–2853, 1999.

[13] H. Ohta, K. Kawamura, M. Orita, M. Hirano, N. Sarukura, and H. Hosono. Current injection emission from a transparent p-n junction composed of p-$SrCu_2O_2$/n-ZnO. *Applied Physics Letters*, 77:475–477, 2000.

[14] A. N. Banerjee and K. K. Chattopadhyay. Nanostructured p-type semiconducting transparent oxides: Promising materials for nano-active devices and the emerging field of transparent nanoelectronics. *Recent Patents on Nanotechnology*, 2:41–68, 2008.

[15] S. Gao, Y. Zhao, P. Gou, N. Chen, and X. Yi. Preparation of $CuAlO_2$ nanocrystalline transparent thin films with high conductivity. *Nanotechnology*, 14(5):538–541, 2003.

[16] L. E. Brus. Electron-electron and electron-hole interactions in small semiconductor crystallites: The size dependence of the lowest excited electronic state. *Journal of chemical physics*, 80:4403–4409, 1984.

[17] T. Dittrich, L. Dloczik, T. Guminskaya, M. C. Lux-Steiner, N. Grigorieva, and I. Urban. Photovoltage characterization of $CuAlO_2$ crystallites. *Applied Physics Letters*, 85:742–744, 2004.

[18] X. G. Zheng, K. Taniguchi, A. Takahashi, Y. Liu, and C. N. Xu. Room temperature sensing of ozone by transparent p-type semiconductor $CuAlO_2$. *Applied Physics Letters*, 85:1728–1729, 2004.

[19] A. N. Banerjee, C. K. Ghosh, S. Das, and K. K. Chattopadhyay. Electro-optical characteristics and field-emission properties of reactive dc-sputtered p-$CuAlO_{2+x}$ thin films. *Physica B*, 370:264–276, 2005.

[20] K. Park, K. Y. Ko, and W. S. Seo. Effect of partial substitution of Ca for Al on the microstructure and high-temperature thermoelectric properties of $CuAlO_2$. *Materials science and engineering*, 129:1–7, 2006.

[21] N. Koriche, A. Bouguelia, A. Aider, and M. Trari. Photocatalytic hydrogen evolution over delafossite $CuAlO_2$. *International Journal of Hydrogen Energy*, 30:693–699, 2005.

[22] R.-J. Xie and N. Hirosaki. Silicon-based oxynitride and nitride phosphors for white leds: A review. *Science and technology of advanced materials*, 8:588–600, 2007.

[23] S. Ye, F. Xiao, Y.X. Pan, Y.Y. Ma, and Q.Y. Zhang. Phosphors in phosphor-converted white light-emitting diodes: Recent advances in materials, techniques and properties. *Elsevier*, 71:1–34, 2010.

[24] D. A. Steigerwald, J. C. Bhat, D. Collins, R. M. Fletcher, M. O. Holcomb, and M. J. Ludowise. Illumination with solid state lighting tech-

nology. *IEEE Journal on selected topics in quantum electronics*, 8(2): 310–320, 2002.

[25] J. K. Sheu, S. J. Chang, C. H. Kuo, and Y. K. Su. White-light emission from near UV InGaN-GaN LED chip precoated with blue/green/red phosphors. *IEEE Photonics Technology Letters*, 15(1):18–20, 2003.

[26] S. Neeraj, N. Kijima, and A. K. Cheetham. Novel red phosphors for solid-state lighting: the system $NaM(WO_4)_{2-x}(MoO_4)_x:Eu^{3+}$, (M : Gd, Y, Bi). *Chemical Physics Letters*, 387(1):2–6, 2004.

[27] Z. Lu and T. Wanjun. Synthesis and luminescence properties of Eu^{3+}-activated $NaLa(MoO_4)(WO_4)$ phosphor. *Ceramics International*, 38: 837–840, 2012.

[28] Y. Ren, G. Zhao, C. Zhang, and Y. Chen. Preparation of $CuAlO_2$ thin films with high transparency and low resistivity using sol-gel method. *Journal of Sol-Gel Science and Technology*, 61:565–569, 2009.

[29] C. K. Ghosh, S. R. Popuri, T. U. Mahesh, and K. K. Chattopadhyay. Preparation of nanocrystalline $CuAlO_2$ through sol-gel route. *Journal of sol-gel science and technology*, 52:75–81, 2009.

[30] P. W. Atkins, T. Overton, J. Rourke, M. Weller, and F. Armstrong. *Inorganic Chemistry*. Oxford University Press, Oxford, UK, 5 edition, 2010.

[31] Ralph G. Pearson. Chemical hardness and density functional theory. *Journal of Chemical Sciences*, 117(5):369–377, 2005.

[32] T. Liu, Y. Xu, and J. Zhao. Low-temperature synthesis of $BiFeO_3$ via PVA sol-gel route. *Journal of the American Ceramic Society*, 93(11): 3637–3641, 2010.

[33] B. J. Ingram and T. O. Mason. Electronic structure and small polaron hole transport of copper aluminate. *Physical Rewiew Letters*, 64 (155114):1–7, 2001.

[34] K. Tonooka, K Shimokawa, and O. Nishimura. Properties of copper-aluminum oxide films prepared by solution methods. *Elsevier*, 411: 129–133, 2002.

[35] S. Götzendörfer, C. Polenzky, S. Ulrich, and P. Löbmann. Preparation of $CuAlO_2$ and $CuCrO_2$ thinfilms by sol-gel processing. *Elsevier*, 518: 1153–1156, 2009.

[36] Z. Deng, X. Zhu, R. Tao, W. Dong, and X. Fang. Synthesis of $CuAlO_2$ ceramics using sol-gel. *Materials Letters*, 61:686–689, 2007.

[37] Y. C. Liou, W. C. Tsai, W. Y. Lin, and U. R. Lee. Synthesis of $Ca_3Co_4O_9$ and $CuAlO_2$ ceramics of the thermoelectric application using a reaction-sintering process. *Journal of the Australasian Ceramic Society*, 44(1):17–22, 2008.

[38] R. S. Yu, C. J. Lu, D. C. Tasi, S. C. Liang, and F. S. Shieu. Phase transformation and optoelectronic properties of p-type $CuAlO_2$ thin films. *Journal of the electrochemical society*, 154(9):838–843, 2007.

[39] K. T. Jacob and C. B. Alcock. Thermodynamics of $CuAlO_2$ and $CuAl_2O_4$ and phase equilibria in the system Cu_2O-CuO-Al_2O_3. *Journal of the American Chemical Society*, 58(5-6):192–195, 1975.

[40] R. Nagarajan, N. Duan, M. K. Jayaraj, J. Li, K. Vanaja, A. A. Yokochi, J. Draeseke, J. Tateb, and A. W. Sleight. P-type conductivity in the delafossite structure. *International Journal of Inorganic Materials*, 3: 265–270, 2001.

[41] J. Tate, H. L. Ju, J. C. Moon, A. Zakutayev, A. P. Richard, J. Russell, and D. H. McIntyre. Origin of p-type conduction in single-crystal $CuAlO_2$. *Physical review B*, 80(165206):1–8, 2009.

[42] T. V. Thu, P. D. Thanh, K. Suekuni, N. H. Hai, D. Mott, and Shinya Koyano, M. Maenosono. Synthesis of delafossite $CuAlO_2$ p-type semiconductor using a nanoparticlebased Cu(i) acetate-loaded boehmite precursor. *Materials research bulletin*, 46:1819–1827, 2011.

[43] W. Lan, M. Zhang, G. Dong, Y. Wang, and H. Yan. Improvement of $CuAlO_2$ thin film electrical conduction by the anisotropic conductivity. *Journal of materials research*, 22:3338–3343, 2007.

[44] M. S. Lee, T. Y. Kim, and D. Kim. Anisotropic electrical conductivity of delafossite-type $CuAlO_2$ laminar crystal. *Applied Physics Letters*, 79:2028–2030, 2001.

[45] D. O. Scanlon, K. G. Godinho, B. J. Morgan, and G W. Watson. Understanding conductivity anomalies in cu-based delafossite transparent conducting oxides: Theoretical insights. *The journal of chemical physics*, 132(024707):1–10, 2010.

[46] H-C. Lu, J.-L. Lu, C.-L. Chu, C.-Y. Lai, and G.-M. Wu. Preparation of nano-powders of p-type transparent conductive copper aluminum oxide by co-precipitation method. In *Nanoelectronics conference*, 2008.

[47] Z. Q. Yao, L. Zhang, C. Q. Zhuang, T. W. Ng, S. L. Liu, M. Vogel, A. Kumar, W. J. Zhang, C. S. Lee, S. T. Lee, and X. Jiang. Energy band engineering and controlled p-type conductivity of $CuAlO_2$ thin films by nonisovalent Cu-O alloying. *Applied Physics Letters*, 100 (062102):1–4, 2012.

[48] P. V. Klevtsov and R. F. Klevtsova. Polymorphism of the double molybdates and tungstates of mono- and trivalent metal with the composition $M^+R^{3+}(EO_4)_2$. *Soviet Powder Metallurgy and Metal Ceramics*, 18:419–439, 1977.

[49] R. D. Shannon. Revised effective ionic radii and systematic studies of interatomic distances in halides and chalcogenides. *Acta Crystallographica Section A*, 32(5):751–767, 1976.

[50] G. Li, L. Li, M. Li, W. Bao, Y. Song, S. Gan, H. Zou, and X. Xu. Hydrothermal synthesis and luminescent properties of $NaLa(MoO_4)_2$:Eu^{3+}, Tb^{3+} phosphors. *Journal of Alloys and Compounds*, 550:1–8, 2013.

[51] Z. Wang, H. Liang, M. Gong, and Q. Su. Luminescence investigation of Eu^{3+} activated double molybdates red phosphors with scheelite structure. *Journal of Alloys and Compounds*, 432:308–312, 2007.

[52] C. Guo, F. Gao, Y. Xu, F. Liang, F. G. Shi, and B. Yan. Efficient red phosphors $Na_5Ln(MoO_4)_4$:Eu^{3+} (Ln : La, Gd, Y) for white leds. *Journal of Physics D: Applied physics*, 42(095407):1–7, 2009.

[53] J. Gu, Y. Zhu, H. Li, X. Zhang, and Y. Qian. Uniform Ln^{3+} (Eu^{3+}, Tb^{3+}) doped $NaLa(WO_4)_2$ nanocrystals: Synthesis, characterization,

and optical properties. *Journal of solid state chemistry*, 183:497–503, 2010.

[54] Z. Wang, H. Liang, L. Zhou, J. Wang, M. Gonga, and Q. Su. $NaEu_{0.96}Sm_{0.04}(MoO_4)_2$ as a promising red-emitting phosphor for LED solid-state lighting prepared by the pechini process. *Elsevier*, 128:147–154, 2005.

[55] G. Blasse and B. C. Grabmaier. *Luminescent materials*. Springer-verlag Berlin Heidelberg, 1994.

[56] A. Konrad, U. Herr, R. Tidecks, and K. Samwer. Luminescence of bulk and nanocrystalline cubic yttria. *Journal of applied Physics*, 90 (7):3516–3523, 2001.

[57] P. F. S. Pereira, A. P. de Moura, I. C. Nogueira, M. V. S. Lima, E. Longo, P. C. de Sousa Filho, O. A. Serra, E. J. Nassar, and I. L. V. Rosa. Study of the annealing temperature effect on the structural and luminescent properties of $SrWO_4$:Eu phosphors prepared by a non-hydrolytic sol-gel process. *Journal of alloys and compounds*, 526:11–21, 2012.

[58] F. B. Cao, L.-S. Li, Z.-J. Wu, X.-R. Wu, J.-H. Zhu, and W.-M. Liu. Preparation of red-emitting phosphor $[K_{0.8}Y_{0.65}Eu^{3+}{}_{0.08}][Mo_{0.2}W_{0.8}O_4]$ and calculation of Eu^{3+} $^5D_0$ quantum efficiency. *Journal of Display Technology*, 8:127–131, 2012.

[59] A. Shalav, B. S. B. S. Richards, and M. A. Green. Luminescent layers for enhanced silicon solar cell performance: Up-conversion. *Solar Energy Materials & Solar Cells*, 91:829–842, 2007.

[60] G. Lakshminarayana and J. Qiu. Photoluminescence of Eu^{3+}, Tb^{3+} and Tm^{3+}-doped transparent SiO_2-Al_2O_3-LiF-GdF_3 glass ceramics. *Journal of Alloys and Compounds*, 476:720–727, 2009.

[61] M. Enculescu, N. Preda, E. Matei, and I. Enculescu. Luminescent micro- and nanofibers based on novel europium phthalate complex. *Materials Chemistry and Physics*, 136:51–58, 2012.

[62] J. Silva, A. Reyes, H. Esparza, H. Camacho, and L. Fuentes. $BiFeO_3$: A review on synthesis, doping and crystal structure. *Integrated Ferroelectrics*, 126(1):47–59, 2011.

[63] S. O. Solopan, O. I. V'yunov, A. G. Belous, T. I. Polek, and A. I. Tovstolytkin. Effect of nanoparticles agglomeration on electrical properties of $La_{1-x}A_xMnO_3$ $(A : Sr, Ba)$ nanopowder and ceramic solid solutions. *Elsevier*, 14(4):501–505, 2012.

[64] Sigma Aldrich. Malonic acid, Des 2012. URL http://www.sigmaaldrich.com/catalog/product/sial/m1296?lang=en&region=NO.

[65] Sigma Aldrich. D-(+)-malic acid, Des 2012. URL http://www.sigmaaldrich.com/catalog/product/supelco/46940u?lang=en&region=NO.

[66] Sigma Aldrich. D-(-)-tartaric acid, Des 2012. URL http://www.sigmaaldrich.com/catalog/product/aldrich/t206?lang=en&region=NO.

[67] T. O. Sunde, E. Garskaite, B. Otter, H. Fossheim, E. R. Saeterli, R. Holmestad, M.-A. Einarsrud, and T. Grande. Transparent and

conducting ITO thin films by spin coating of an aqueous precursor solution. *Journal of Materials Chemistry*, 22(31):15740–15749, 2012.

[68] M. L. Fontaine, C. Laberty-Robert, A. Barnab, F. Ansart, and P. Tailhades. Synthesis of $La_{2-x}NiO_{4+d}$ oxides by polymeric route: Non-stoichoimetry control. *Ceramics International*, 30(8):2087–2098, 2004.

[69] L. Zhang. Preparation of multi-component ceramic nanoparticles. Technical report, The Ohio state university, 2004.

[70] H. Zhao, M.-A. Einarsrud, and F. Vullum-Bruer. High capacity nanostructured $Li_2Fe_xSiO_4$/C with Fe hyperstoichiometry for Li-ion batteries. *Journal of power sources*, 235:234–242, 2013.

[71] S. Zumdahl and S. Zumdahl. *Chemistry*. Charles Hartford, 2010.

[72] A. L. Patterson. The Scherrer formula for X-ray particle size determination. *Physical Review Letters*, 56:978–982, 1939.

[73] S. Brunauer, P. H. Emmett, and E. Teller. Adsorption of gases in multimolecular layers. *Journal of the american chemical society*, 60: 309–319, 1938.

[74] M. Rotan. *Phase composition, microstructure and resistance to attrition of alumina-based supports for Fischer-Tropsch catalysts*. PhD thesis, Norwegian University of Science and Technology, Faculty of Natural Sciences and Techology, Department of materials science and engineering, 2012.

[75] G. E. Lloyd. Atomic number and crystallographic contrast images with the sem: a review of backscattered electron techniques. *Mineralogical Magazine*, 51:3–19, 1987.

[76] S. Weber. *Spray pyrolysis of thermal barrier coatings*. PhD thesis, Norwegian university of science and technology, 2012.

[77] T. Mokkelbost, I. Kaus, T. Grande, and M.-A. Einarsrud. Combustion synthesis and characterization of nanocrystalline CeO_2-based powders. *Chemistry of materials*, 16:5489–5494, 2004.

[78] B. Klingenberg and M. A. Vannice. Influence of pretreatment on lanthanum nitrate, carbonate and oxide powders. *Chemistry of Materials*, 8:2755–2768, 1996.

[79] K. Nakamoto. *Infrared and Raman spectra of inorganic and coordination compounds*. John Wiley & Sons, Inc., 1997.

[80] R. Krishnan, J. Thirumalai, I. B. S. Banu, and J. Peter. Rugby-ball-shaped $Na_{0.5}La_{0.5}MoO_4$:Eu^{3+}: 3d architectures: synthesis, characterization, and their luminescence behavior. *Journal of nanostructure in chemistry*, 3(14):1–5, 2013.

[81] B. D. Dalvi and A. M. Chavan. Thermal decomposition of mixed oxalates. *Journal of Thermal Analysis and Calorimetry*, 14:331–334, 1978.

[82] *Ethylene glycol product guide*. MEGlobal, 2008.

[83] M. L. V. Ramires, C. A. Nieto de Castro, Y. Nagasaka, A. Nagashima, M. J. Assael, and W. A. Wakeham. Standard reference data for the thermal conductivity of water. *Journal of physical and chemical reference data*, 24:1377–1381, 1994.

[84] *MSDS Tartaric acid*. International Programme on Chemical Safety and the European Commission.

[85] A. Daneshfara, M. Baghlanib, R. S. Sarabib, R. Sahraeia, S. Abassia, H. Kaviyana, and T. Khezeli. Solubility of citric, malonic, and malic acids in different solvents from 303.2 to 333.2 k. *Fluid phase equilibria*, 313:11–15, 2012.

[86] R. F. Harrington. *Introduction to Electromagnetic Engineering*. McGraw-Hill, 1958.

[87] *Dense shaped refractory products - determination of bulk density, apparent porosity and true porosity*. The international organization for standardization, 2 edition, July 1998.

Appendix

A Standardization of precursor solutions

The method described in the scheme below has been used. The cations Mo^{6+} and Cu^{2+} were not a part of the original document and has been included by the author of this report.

TERMOGRAVIMETRISK STANDARDISERING AV KATIONLØSNINGER

Det skal utføres fire paralleller av hver løsning når de standardiseres.

Forskjellige kation skal standardiseres ved forskjellige temperaturer:

500 °C	Mo
700 °C:	Mn, Ni
800 °C:	Ca, Co, Fe, La, Mg, Nb, W, Cu
1000 °C:	Al, Ce, Ga, Gd, Ti, Yb
1200 °C:	Ca-acetat, Y, Zr

Temperaturprogram:

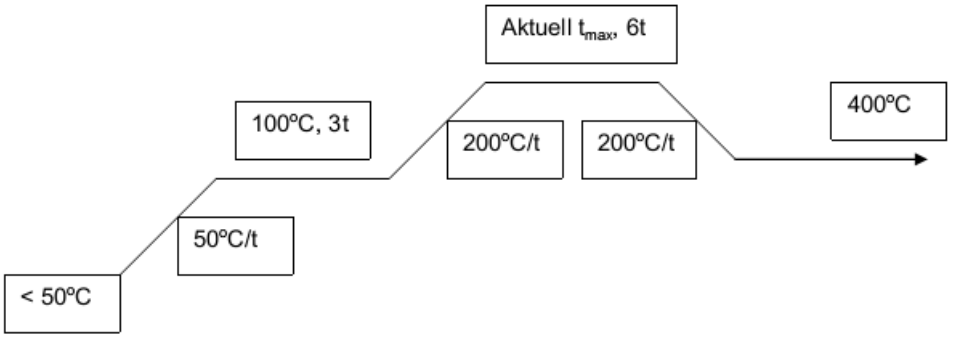

NB! Ba, K, Na og Sr standardiseres ikke, da disse nitratene er uten krystallvann. Tørkes ved 200 °C i 24 timer og veies inn direkte ved bruk!

Det brukes digler som er forhåndsglødet ved aktuell temperatur, eller varmere, med en liten dott CaO-ull oppi. Dette for å hindre koking.

Diglene veid tomme før det blir hatt nitratløsning i dem og de blir veid igjen. Mengde nitratløsning i digelen er vanligvis ca 2 ml. Etter denne veiingen blir så diglene med løsningen satt i ovnen til en ny varmebehandling. Diglene blir varmet forsiktig (50 °C/h) opp til 100 °C og holdt der i tre timer. Dette for å unngå kraftig koking med tap av masse. Deretter varmes de videre med 200 °C/h til aktuell temperatur som er avhengig av nitratet som skal dekomponeres. Holdetid på maks temperaturen er typisk 6 timer. Diglene blir så avkjølt med 200 °C/h ned til 400 °C og holdes der til de tas ut av ovnen . Den siste avkjølingen skjer i eksikator før diglene veies.

Ut fra vekten av nitratløsningen og det resulterende oksidet bestemmes konsentrasjonen til utgangsløsningen i mol kation/gram løsning. Det er laget regneark i Excel til dette. Standardavviket på de fire parallellene bør ikke være større enn i størrelsesorden 10^{-7}.

Om man er usikker på om en standardiseringstemperatur er korrekt, kan dette sjekkes ved å ta opp XRD spekter av gløderesten og se om det er et rent oksid man har fått.

20.11.2007
Rune T. Barland

B Conductivity measurements

The conductivity of the pellets for batch 2 and 3 was found by simple resistance measurements using a multimeter as current could not be passed through them due to high contact resistance between the silver paint and the pellet surface. The resistivity was then calculated from the measured resistance using the dimensional values of the pellets in Table B.1. Four contacts, two long contacts and two short contacts, were painted on the

pellets using silver paint using the layout in Figure B.1. The resistance values are given in Table B.2.

Table B.1: *The dimensions of the pellets as presented in Figure B.1. The values are given in millimeters.*

	Batch 2			Batch 3	
Pellet no.	**1**	**2**	**3**	**1**	**2**
a	4.0	3.5	5.0	5.0	4.0
b	1.0	0	1.0	2.0	1.0
c	6.0	6.0	5.0	6.0	6.0
d	3.0	1.5	2.0	2.5	2.5
e	0.5	1.0	1.0	1.0	1.0

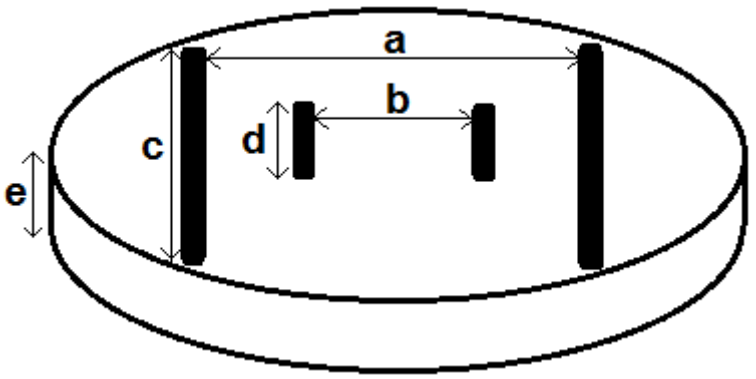

Figure B.1: *The layout of the silver paint contacts on the pellets. The values of a, b, c, d and e are found in Table B.1.*

Table B.2: *The resistance measured between the current contacts and voltage contacts of the pellets. The values denoted with the letters l and s are between the long contacts and short contacts , respectively. Three pellets were successfully made from batch 2 and two pellets were made from batch 3. All the values are in kΩ.*

Pellet no.	Batch 2	Batch 3
1	444^{l}	81.3^{cl}
	870^{s}	118.4^{s}
2	551^{l}	158.5^{l}
	Short-circuit^{s}	708^{s}
3	196^{l}	
	1.62^{vs}	

By using the lowest resistance value for each batch, thus minimizing the contribution from the contact resistance, the resistance for the two batches was calculated by using the Equation 6 [86],

$$\rho = \frac{R \cdot A}{l} \tag{6}$$

where ρ is the resistivity, R is the resistance, A is the area of the cross-section where the current passes through and l is the length of this current path.

C Density calculations with Arkimedes' method

The density of the pressed and sintered pellets was found by using Arkimedes' method. The method can be used for calculating bulk density, apparent porosity and true porosity of bulk materials. First, the mass of the dry

sample, m_d, was measured before it is immersed into isopropanol or some other suitable liquid with known density. The apparent mass in immersed state, m_i, was then measured before the sample was removed from the liquid and the mass of the completely wet sample, m_w, was measured. The bulk density of the sample could now be calculated by Equation 7 [87],

$$\rho_b = \frac{m_d}{m_w - m_i} \cdot \rho_l \tag{7}$$

where ρ_l is the density of the liquid the sample is immersed into.